

AD-A057 939

SPERRY UNIVAC ST PAUL MINN DEFENSE SYSTEMS DIV
COMPOSITE THIN FILM PILOT PLANT.(U)

F/6 11/6

JAN 78 R H DEAN, R D MORRISON, E J TOROK

DAA053-76-C-0164

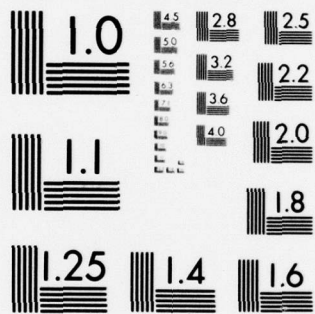
UNCLASSIFIED

UNIVAC-DSD-PX-12492

NL

| OF |
AD
A057939





MICROCOPY RESOLUTION TEST CHART
NATIONAL BUREAU OF STANDARDS-1963-A

ADA057939

AD No. _____
DDC FILE COPY

LEVEL *(1)*

T2
SC

UNIVAC DSD Report No. PX 12492

COMPOSITE THIN FILM PILOT PLANT

Final Technical Report

R. H. Dean, R. D. Morrison, E. J. Torok

Sperry Univac
P.O. Box 3525
St. Paul, MN 55165

January 31, 1978

Final Report For Period July 76 - January 78

Contract No. DAA033-76-C-0164

Prepared For:

U. S. Army Mobility Equipment
Research and Development Command
Fort Belvoir, Virginia 22060

DDC
UNCLASSIFIED
EXEMPT FROM GDS
F

APPROVED FOR PUBLIC RELEASE; DISTRIBUTION
UNLIMITED

78 05 00 100

LEVEL II

12

UNIVAC DSD Report No. PX 12492

6

COMPOSITE THIN FILM PILOT PLANT.

Final Technical Report

10

R. H. Dean, R. D. Morrison E. J. Torok

Sperry Univac
P.O. Box 3525
St. Paul, MN 55165

January 31, 1978

12 78 p.

11 31 Jan 78

Final Report for Period July 76 - January 78

Contract No. DAAG53-76-C-0164

15

Prepared For:

U. S. Army Mobility Equipment
Research and Development Command
Fort Belvoir, Virginia 22060

9 Final rept. Jul 76-Jan 78

14 UNIVAC-DSD-PX-12492

DISTRIBUTION STATEMENT A

Approved for public release
Distribution Unlimited

78 08 09 100 alt
408 125

DISPOSITION INSTRUCTIONS

Return this report to Materials Engineering Division, VRDME-VL, U. S. Army Mobility Equipment Research and Development Command Fort Belvoir, Virginia, 22060 when no longer needed.

DISCLAIMERS

The findings in this report are not to be construed as an official Department of the Army position unless so designated by other authorized documents.

When Government drawings, specifications, or other data are used for any purpose other than in connection with a definitely related Government procurement operation, the United States Government thereby incurs no responsibility nor any obligation whatsoever; and the fact that the Government may have formulated, furnished, or in any way supplied the said drawings, specifications, or other data is not to be regarded by implication or otherwise as in any manner licensing the holder or any other person or corporation, or conveying any rights or permission, to manufacture, use, or sell any patented invention that may in any way be related thereto.

ACCESSION for	
NTIS	Write Section <input checked="" type="checkbox"/>
DDC	B R Section <input type="checkbox"/>
UNANNOUNCED	<input type="checkbox"/>
JUSTIFICATION	
BY	
DISTRIBUTION/AVAILABILITY CODES	
D.	SPECIAL
A	

SECURITY CLASSIFICATION OF THIS PAGE (When Data Entered)

REPORT DOCUMENTATION PAGE		READ INSTRUCTIONS BEFORE COMPLETING FORM								
1. REPORT NUMBER PX-12492 ✓	2. GOVT ACCESSION NO.	3. RECIPIENT'S CATALOG NUMBER								
4. TITLE (and Subtitle) Composite Thin Film Pilot Plant Final Technical Report		5. TYPE OF REPORT & PERIOD COVERED Final Technical July '76 - Jan '78								
7. AUTHOR(s) R. H. Dean, R. D. Morrison, E. J. Torok		6. PERFORMING ORG. REPORT NUMBER								
9. PERFORMING ORGANIZATION NAME AND ADDRESS Sperry Univac ✓ P.O. Box 3525 St. Paul, MN 55165		8. CONTRACT OR GRANT NUMBER(s) DAAG53-76-C-0164 ¹⁰								
11. CONTROLLING OFFICE NAME AND ADDRESS U.S. Army Mobility Equipment Research & Development Command Fort Belvoir, Virginia 22060		10. PROGRAM ELEMENT, PROJECT, TASK AREA & WORK UNIT NUMBERS A002 DD Form 1423								
14. MONITORING AGENCY NAME & ADDRESS (if different from Controlling Office)		12. REPORT DATE January 31, 1978								
		13. NUMBER OF PAGES								
		15. SECURITY CLASS. (of this report)								
		15a. DECLASSIFICATION/DOWNGRADING SCHEDULE								
16. DISTRIBUTION STATEMENT (of this Report)										
17. DISTRIBUTION STATEMENT (of the abstract entered in Block 20, if different from Report)										
18. SUPPLEMENTARY NOTES										
19. KEY WORDS (Continue on reverse side if necessary and identify by block number)										
<table border="0"> <tr> <td>Vacuum deposition</td> <td>Titanium-Aluminum</td> </tr> <tr> <td>Thin Films</td> <td>Silicon Carbide-Aluminum</td> </tr> <tr> <td>Composites</td> <td>Alumina-Aluminum</td> </tr> <tr> <td>Aluminum</td> <td>Internal Clamp</td> </tr> </table>			Vacuum deposition	Titanium-Aluminum	Thin Films	Silicon Carbide-Aluminum	Composites	Alumina-Aluminum	Aluminum	Internal Clamp
Vacuum deposition	Titanium-Aluminum									
Thin Films	Silicon Carbide-Aluminum									
Composites	Alumina-Aluminum									
Aluminum	Internal Clamp									
20. ABSTRACT (Continue on reverse side if necessary and identify by block number)										
<p>Tooling was designed and fabricated for the high rate vacuum deposition of alternating superimposed layers of high and low modulus materials. A continuous metal belt substrate was passed over adjacent electron beam and resistance heated sources. Composite films of titanium-aluminum, silicon carbide-aluminum and alumina-aluminum, were fabricated, removed from the substrate and their ultimate tensile strengths determined. Tensile strengths a number of times bulk values were obtained for the titanium-aluminum films which exhibited</p>										

DD FORM 1473
1 JAN 73

EDITION OF 1 NOV 65 IS OBSOLETE

SECURITY CLASSIFICATION OF THIS PAGE (When Data Entered)

the highest ultimate tensile strength. The ultimate tensile strength was determined using an internal clamp technique which was analyzed empirically and theoretically.

The composite film as deposited is crystalline, biaxial and isotropic. The significance of this is that:

a. It has a very high potential for modulus of elasticity.

b. When plied as a sheet into a laminate, it does not have to be rotated to achieve isotropicity in the manner that woven cloths must be rotated. When compared to fibers, the film thus has an almost 2X advantage with regard to tensile strength.

A maximum tensile strength of 540,000 psi was obtained for a titanium-aluminum composite 0.144×10^{-3} inches thick, comprised of approx 730 60 Angstrom layers.

For alumina-aluminum a maximum tensile strength of 280,000 psi was obtained on a composite 0.480×10^{-3} inches thick made up of approx 190 alternate layers of aluminum (1200 Å thick) and alumina (104 Å).

The aluminum represents 92% of the film pair. At 1200 Å the strength is approximately 60,000 psi. On this basis the strength of the alumina was over 2,800,000 psi.

For a silicon carbide-aluminum composite 0.50×10^{-3} inches thick comprised of approx 230 alternate layers of aluminum (930 Å) and silicon carbide (170 Å), a maximum tensile strength of 67,000 psi was obtained.

For an aluminum film 1.0×10^{-3} inches thick with an unknown number of flash evaporated layers the maximum tensile strength was 81,000 psi.

Moduli of elasticity were not significantly changed.

Foreward

This report was prepared by Sperry Univac, Physical Sciences Department, Univac Park, St. Paul, Minnesota under Contract Number DAAG53-76-C-0164

Laboratory personnel who participated are:

R. H. Dean (Project Engineer), R. J. Engfer, D. D. Long
R. D. Morrison, C. J. Nelson and E. J. Torok.

S. J. Lins

Manager, Physical Sciences Department

Sperry Univac

St. Paul, MN 55165

Sol Goldfein

Project Monitor

Mobility Equipment Research and Development Command

Fort Belvoir, VA 22060

Table of Contents
Final Technical Report

1.0	Introduction
2.0	System Description
2.1	Sources and Power Supplies
2.3	Wire Feeds
2.4	E-beam Operation
2.5	Substrate Transport
3.0	Composite Thin Film Deposition Process
3.1	Checkout Before Closing
3.2	Close Chamber
3.3	Pumpdown
3.4	Hookup Before Evaporation
3.5	Evaporation
3.6	Open System
3.7	Vacuum System Checklist
3.8	Film Removal
3.9	Heat Transfer
4.0	Material Selection for Composite Deposition
4.1	Modulus of Elasticity in Tension
4.2	Specific Stiffness
4.3	Alternate Material Deposition
5.0	Mechanical Properties - Experimental Methods
5.1	Analysis of the Internal Clamp Method
5.2	Results of Mechanical Measurements
5.3	Film Properties - Resistance
6.0	Conclusions
7.0	Recommendations
	Appendix A
	Stress Distribution Analysis
	Appendix B
	Distribution of Report

1.0 INTRODUCTION

The overall objective of this multiphase program is the exploitation of the phenomenon of very high strength exhibited by materials in thin film form. This program attempts to fabricate a planar layered composite which would then be used as the high strength member in a second or hybrid composite. A planar reinforcement, e.g., high strength film, would be bidirectional as opposed to fibrous reinforcement when the fibers are parallel. Thus, whereas the strength of fibrous reinforcement must be reduced in strength twice in order to obtain a working isotropic laminate (fiber-cloth-resin matrix laminate), the film goes directly to the laminate (film-resin matrix-laminate). In a direct comparison of fiber and film, therefore, the film would have approximately 2X the strength potential that a fiber would have.

This is Phase II of a multiphase program. Phase I was a design study, R.H. Dean et.al, Titanium-Aluminum-Ultra-Thin-Film Study, MERADCOM contract No. DAAK02-75-C-0036. The objective of phase I was the development of a production method for fabricating a thin film composite.

The primary objective of phase II has been the development and fabrication of a composite thin film deposition pilot plant capable of relatively high deposition rates.

Multilayered composites were fabricated. The composites consisted of alternate-superimposed layers of low and high modulus materials. Aluminum (1000 series) served in all cases as the low modulus member of the material pair. High modulus members were titanium, silicon carbide and alumina.

The high modulus materials were chosen based on their potential physical properties. Material cost is also an important consideration since planar reinforcements must compete with existing technologies.

Physical testing of the multilayered composites was subcontracted to the Engineering Experiment Station of Georgia Institute of Technology. Tests were performed by or under the direction of Dr. E. R. Livesay. Analysis of the internal clamping method was done by Lt. George Lucas of MERADCOM using a photoelastic technique to determine effective specimen widths and using SEM examinations to provide substantially more accurate measurements of specimen thicknesses.

2.0 System Description

The vacuum system is equipped with a 10" oil diffusion pump and a liquid nitrogen cold trap. A 53 CFM roughing pump also serves as the foreline pump. The pumps evacuate through a port in the backside of the upper chamber. The vacuum chamber consists of an upper rectangular box chamber with interior dimensions 24" x 32" x 36" high which is open at the bottom. The lower chamber interior is 23.5" x 25" x 16.5" high. A rectangular baseplate 28" x 36" is welded to the top of the lower chamber and is fitted with a recessed "O" ring which forms a vacuum seal between the mating surfaces of the two chambers. See Figures 1 and 2. The opening in the lower chamber is then common to both chambers.

An ultimate pressure of 2×10^{-6} Torr was attainable with all the tooling installed. The lower chamber was designed to support the substrate transport superstructure and to hold the sources for the vapor deposition of the composite films. Two viewing ports made possible the observation of the sources and wire feeds during deposition. The chamber was water cooled on the four sides and bottom via stainless steel channel welded on the exterior chamber walls. Power supplies had the capability of a total power input of 26 KW into this relatively small chamber. The necessity of cooling the chamber as well as the tooling is obvious. Cooling lines which were plumbed from inlet and outlet cooling water manifolds are listed

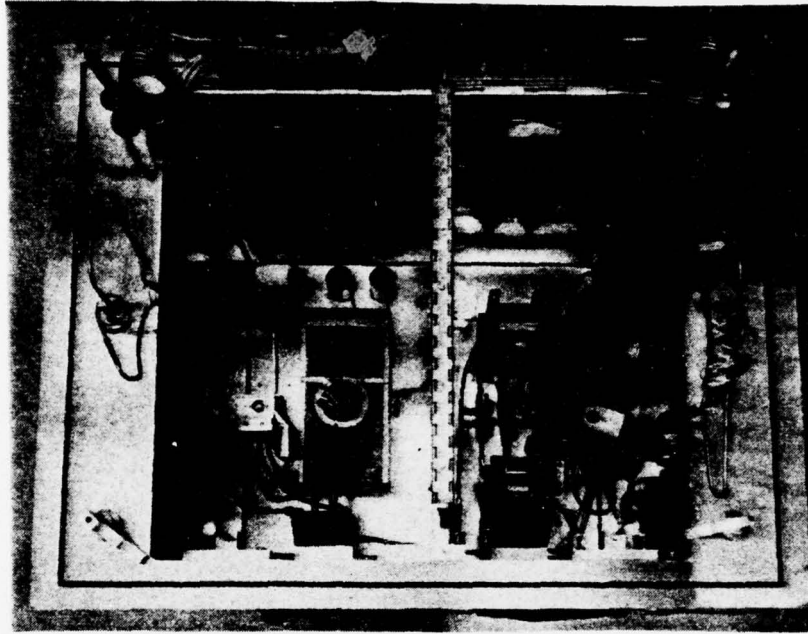


Figure 1. Substrate transport tipped back and shutter dropped exposing tooling installed in source chamber. The electron beam hearth is left center. Two resistance heated boats and the aluminum wire feeds are mounted in the right side.

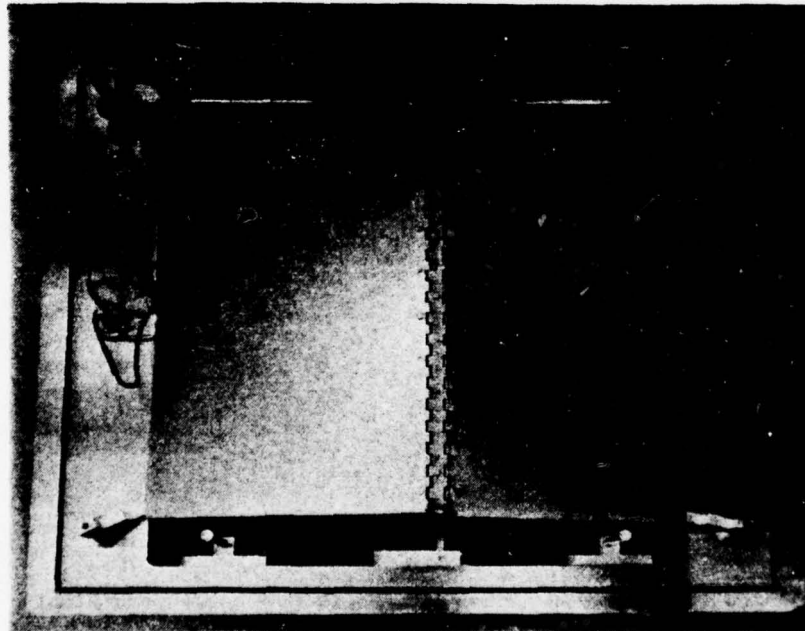


Figure 2. Shutters closed. The three crystal rate monitor sensors "see" the sources through cutouts in the shutters.

below. The cooling lines were coded as shown.

Water In	Water Out	Tooling
0 - 0	10 - 10	three cold plates (substrate cooling)
1 - 1	11 - 11	lower chamber walls
2 - 2	12 - 12	mounting blocks for boats
3 - 3	13 - 13	aluminum wire feeds
4 - 4	14 - 14	mounting blocks for boats
5 - 5	15 - 15	titanium wire feed
6 - 6	16 - 16	aluminum crystals (rate monitor)
7 - 7	17 - 17	titanium crystal (rate monitor)

These lines made up an umbilical cord from the water manifolds to the lower chamber. The water lines were not disconnected when raising, lowering or retooling the chamber. Water flow, indicators on the system console were lit when a minimum water flow was present to cool the diffusion pump, the boat mounting blocks, the rate monitor crystal oscillators, the wire feeds, and the chamber.

Additional water cooling was provided for the walls of the upper chamber, the high current feed-throughs and the e-beam hearth. The water flow for the hearth was interlocked with the e-beam power supply.

2.1 Sources and Power Supplies

A 3" dia e-beam hearth with a 20 KW rating was centered in one side of the lower chamber. See Figure 1. A 16 KW power pack with automatic X - Y deflection (beam sweep) supplied the hearth input power. This source was used for the deposition of titanium, alumina, carbon, and silicon carbide.

The boat selected for aluminum evaporation was the UCAR grade HDA which is an intermetallic composite of boron nitride and titanium diboride.

Two of these boats were mounted in the lower chamber and were separated from the titanium deposition area by a vertical shield. The input power to each boat was supplied by an autotransformer associated with two 2500 VA high current transformers in parallel. Therefore each boat had available 5000 VA. A single boat per power supply gives the best economics in terms of boat life.¹

1 Hedge, John B. and Bagot, William A. "Power Parameters of Metallizing Boats" R/D Dec. '71 Vol. 22 No. 12 p. 36

2.2 Boat Operation

The boats were press-fit into machined slots in copper mounting blocks with an intervening layer of graphite tape. The mounting blocks were water cooled and the thermal expansion of the boats (confined in the slots) resulted in excellent electrical contact. This mounting method permits linear thermal expansion of the boat and proved to be relatively trouble free.²

The slots in the mounting blocks must be aligned to avoid subjecting the boat to a mechanical stress when it is press-fit into place. The maximum operating temperature of the HDA boat is 1600°C. This is referred to as the cracking temperature. If the boat temperature exceeds 1600°C the boat will begin to decompose and an increase in system pressure will be noted.

Once a crack in a boat begins to develop, the effective cross-sectional area at that point is reduced. The resistance increases and the evaporation rate decreases. When the current is again raised, a hot spot occurs at the crack and the decomposition of the boat continues until the boat is "open".

Two identified causes of boat cracking are: (1) subjecting it to a mechanical stress and (2) energizing it under high current conditions while the boat is "dry".

2 Baer, Charles A. "Vacuum Metallizing" R/D Feb. '74. p.54

A decreasing rate and lower boat current are indicative of (1) a malfunctioning wire feed or (2) the initiation of a crack in a boat.

In a flooded condition, low rate and high current conditions exist. Evaporant feeding would be halted until the rate recovered. At times a flooded boat drew more than 500 amperes without developing a sufficient rate to remove the excess evaporant.

After removing a flooded boat from the vacuum system, the excess aluminum could be peeled from the four sides of the boat. A file was used to abrade through the aluminum along the edges and a blade was forced between the surfaces of the boat and the excess aluminum. The boat could then be reloaded into the mounting blocks by replacing the graphite tape and pressing it into place.

Aluminum rates were easy to control. The rate could be increased by increasing the feed rate of the aluminum wire. The current would also increase because of the lower impedance. The boat operation is best described as a constant feed flash evaporation.

Typically the aluminum sources were operated at 300 amperes 9 VAC with a feed rate of 0.66 g/min/boat. The maximum feed rate was 2.35 g/min/boat (282 g/hr/2 boats).

Splatter (Aluminum)

The plumbing within the vacuum system was simplified by removing several rubber connectors in the mounting block cooling lines and replacing them with copper tubing. These connectors had been the source of several water leaks. One end of mounting block of each boat was made common with electrical ground through the copper water cooling lines.

The wire feeds were also at ground potential and whenever the aluminum wire contacted the boat arcing was visible at the point of contact. Aluminum splatter was severe. This condition was corrected by again isolating the boat power supplies from electrical ground which eliminated the aluminum feedwire as a current path.

2.3 Wire Feeds

High torque variable speed DC gearmotors were used to directly drive the wire feeds. The motors were mounted under the lower chamber and were used in conjunction with FerrofluidicTM feed-throughs. A collar around the OD of the feed-through served as a mount for the wire feed. The feed mechanism consisted of two knurled rollers, one driven and one idler. Tension on the idler was adjustable with set screws. The wire was fed directly over one end of the boat. During deposition the wire seldom touched the boat or melt. The radiant heat from the source would melt (and degas) the aluminum wire and it would drip onto the boat. The wire feed nozzles were too close to the aluminum sources and occasionally they would

Trademark Ferrofluidic Corp.

become clogged with aluminum condensation which would result in wire feed malfunction. Because the large capacity of the e-beam hearth it proved unnecessary to wire feed the titanium source during deposition.

2.4 E-beam Operation

The e-beam hearth was the permanent magnet type. The crucible had a volume of 157cc. The voltage from the power supply was adjustable from 4 to 10 KV. However, all depositions were accomplished at 10 KV and power input was controlled by adjusting the emission current.

The e-beam was not operated until system pressure was in the range 2×10^{-5} Torr. The beam could be observed on the source material in the hearth with a power input of 500 watts.

The emission current was increased slowly and the X - Y sweep controls were adjusted to increase spot size while maintaining the spot centered in the hearth.

Source materials degassed and system pressure increased initially. All the source materials with the exception of titanium contributed to the system gas load.

Tooling located in an e-beam deposition chamber must be grounded to prevent the build-up of static charges. Ungrounded fixtures

can acquire static charges equivalent to the high voltage output of the power supply (10 KV). The beam must never be operated into an empty hearth. The hearth must be loaded and cooled or damage will result. Cooling water for the power supply and the hearth must be interlocked with the power supply.

Splatter (Titanium)

The hearth of an e-beam source and its wire feed are both at electrical ground potential. Splatter caused by the feedwire being a current path would not be expected.

Because of the large capacity of the e-beam hearth it was not necessary to wire feed this source during a run. Chunks of titanium were added to the hearth when the system was retooled between runs.

Titanium splatter was apparent if these chunks were not totally melted prior to opening the shutter. The splatter was believed due to a gas load in the source material. The splatter or spitting was eliminated by achieving a total melt before dropping the shutter.

2.5 Substrate Transport

The substrate transport superstructure was made up of the following components:

- (1) four 8" diameter aluminum drive rollers
- (2) three substrate cooling plates
- (3) frame and supports
- (4) substrate tension arm and tension roller
- (5) 1/3 HP permanent magnet drive motor
- (6) drive chain, sprockets and bearings.

See Figure 3.

The superstructure was hinged to the lower chamber and could be tipped back for retooling between deposition runs. All four drums were chain driven. Bearings and chains were coated with a dry lubricant, tungsten disulfide. The DC motor was adapted to the vacuum environment. The bearings were degreased and were lubricated with the WS_2 . All paint was removed. The insulation on the armature leads was stripped and replaced with flexible glass sleeving. In this way the gas load contribution of the motor was greatly reduced. The mounting of the motor within the vacuum system made possible direct drive of the substrate transport and simplified the transport design.

The power requirements for the motor were minimal and no problems were encountered with overheating even during deposition runs in which the drive motor was energized up to 40 minutes.

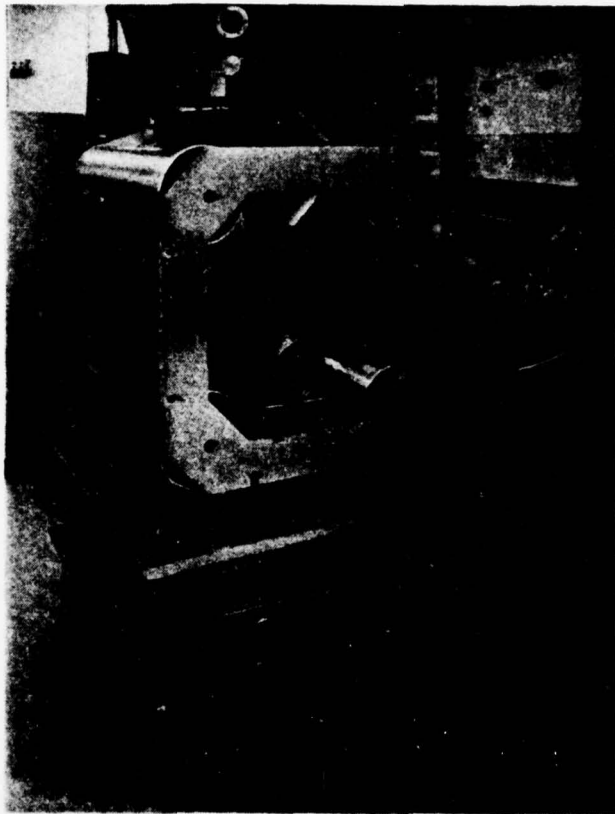


Figure 3. Lower vacuum chamber and substrate transport superstructure.

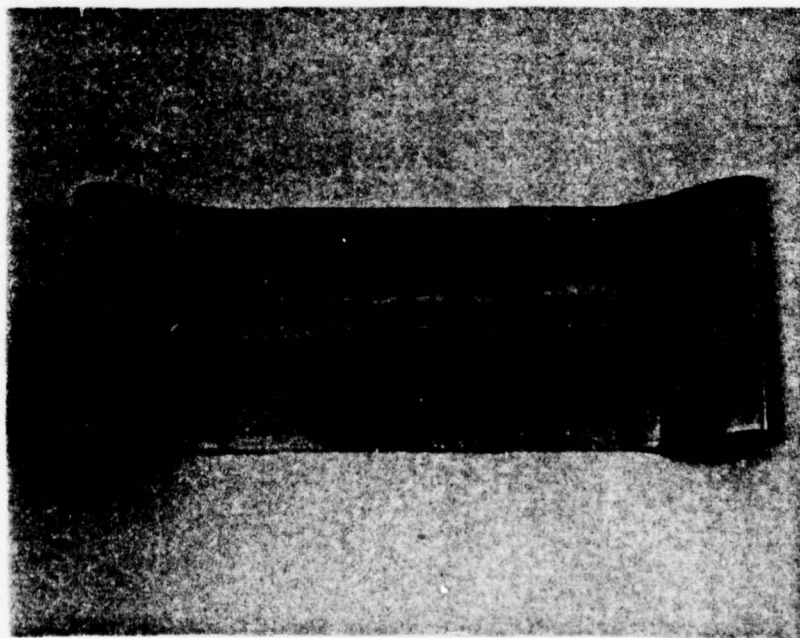


Figure 4. Substrate belt.

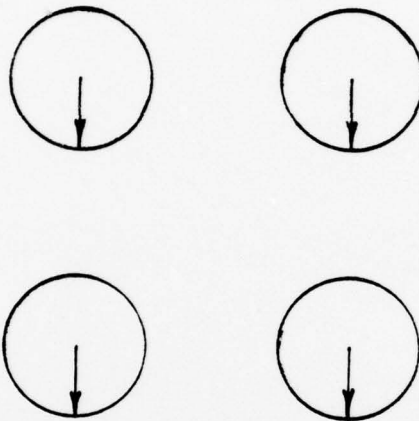
The motor mount was adjustable for the purpose of setting drive chain tension.

The cold plates also served as supporting members of the superstructure frame. Each cold plate consisted of two matched 1/4" aluminum plates which compressed a soft copper cooling line between them. The cooling line was preformed in a serpentine pattern. Both water and liquid nitrogen were used as coolants. When liquid nitrogen was used, the system pressure improved because the cold plates effectively "pumped" water vapor.

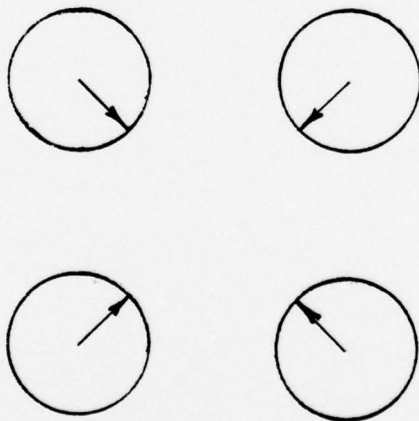
The substrate was a single 20" wide 0.003" thick endless steel belt. The belt was about 9 feet long and approximately 24 inches of its length were exposed to the sources. See Figure 4. The tension idler roller maintained the substrate in contact with the drive rollers. All four drive rollers were chain driven; the substrate was friction driven. See Figure 3. The substrate was removed by tipping the hinged substrate transport superstructure back approximately 90°, releasing the springs on the tension roller, and lifting the substrate clear of the superstructure.

The drive rollers, because of their mass and relatively good substrate contact, act as heat sinks for the substrate.

The drive rollers were not balanced and when the substrate transport was tested the entire vacuum system shook. This occurred because the imbalance of the four rollers was in phase when the drive chain was connected.



The drive rollers were realigned as below and the vibration subsided.



3.0 Composite Thin Film Deposition Process

3.1 Checkout Before Closing

Refer to Vacuum System Checklist (3.7).

3.2 Close Chamber

The lower chamber, which with tooling weighs approximately 500 pounds, is moved with the aid of an electro hydraulic lift fork into position under the upper chamber. The roller guide blocks are aligned with "T" guide bars and the chamber is slowly raised until the chambers mate. A "C" clamp safety mechanism is engaged. The lift fork is maintained in position until the chamber is roughed down. Atmospheric pressure holds the lower chamber in position when the system is evacuated.

See Figure 5.

3.3 Pumpdown

Typical vacuum procedures apply. The system is pressure protected and the high vacuum valve is automatically closed if the chamber pressure increases to a predetermined set point.

3.4 Hookup Before Evaporating

Refer to vacuum system check list (3.7).

3.5 Evaporation

1. System is on high vacuum.
2. If liquid nitrogen (LN) is to be used in cold plates, cooling is begun $\frac{1}{2}$ hour prior to evaporation.
3. Check interlock lights on e-beam supply: water flow, magnet current (e-beam hearth), vacuum, and system closed.
4. Check water flow indicators on system console. Adjust flow if required.
5. Bake out or degas any new boats or GrafoilTM used in the aluminum sources. Observe system pressure as current is increased to 200 amps (1.8 KW). System pressure should rise and rapidly recover.
6. Observe titanium source through port in chamber. Use eye protection for u-v radiation. Confirm beam is positioned on source. Pre-melt any chunk titanium added to e-beam hearth (8 KW). Reduce power input to 3.5 KW until shutter is opened.
7. Observe boats through chamber port. Increase power input on each boat (2.5 KW) until preloaded aluminum is melted and an increasing rate is observed on its respective rate monitor. Energize wire feeds. Rates should increase rapidly and stabilize.

Note: Do not leave boats energized at higher inputs if the wire feed is inoperative.
8. Energize substrate transport drive motor. Motor speed may be determined through port in upper chamber.
9. Adjust titanium and aluminum rates if required.

Trade Mark Union Carbide

10. Open shutter. Record time.
11. When desired thickness has been deposited, de-energize sources and feeds. Close shutters. Record time. Shut off cold plate LN.
12. De-energize transport motor.

3.6 Open System

Note: If LN has been used in cold plates, they must be warmed up prior to opening system or condensation will occur.

1. High vacuum valve is closed. Ion gauge off.
2. Power supplies, LN, rate monitors and vacuum interlock are disconnected from lower chamber base plate.
3. Lift fork is repositioned to support chamber.
4. "C" clamp safety mechanism is disengaged.
5. System vent valve opened.
6. Chamber is lowered for film removal and retooling.

3.7 Vacuum System Checklist

BEFORE CLOSING

- SYSTEM CLEANED
- E-BEAM CRYSTAL REPLACED
- E-BEAM CRYSTAL CHECKED
- FRONT Al CRYSTAL REPLACED
- FRONT Al CRYSTAL CHECKED
- REAR Al CRYSTAL REPLACED
- REAR Al CRYSTAL CHECKED
- PORT SHIELDS IN
- E-BEAM LEAD SHIELDS IN
- FRONT Al FEED CHECKED
- REAR Al FEED CHECKED
- AL STARTER WIRE IN BOATS
- E-BEAM MIRROR REPLACE & POSITION
- FRONT BOAT MIRROR REPLACE & POSITION
- REAR BOAT MIRROR REPLACE & POSITION
- HIGH VOLTAGE SHORT TEST
- FILAMENT CONTINUITY
- FRONT BOAT CONTINUITY
- REAR BOAT CONTINUITY
- BOAT TO GROUND SHORT TEST
- E-BEAM HEARTH LOADED
- Al FEEDS - ENOUGH WIRE
- COLD PLATE FEEDTHRU TIGHT
- O-RING CLEAN
- LEAK TEST NEW PLUMBING
- SHUTTER POSITIONED

BEFORE EVAPORATING

- Al SOURCE WATER ON
- E-BEAM WATER ON
- REAR Al POWER SUPPLY CONN.
- FRONT Al POWER SUPPLY CONN.
- E-BEAM CRYSTAL CONN.
- FRONT Al CRYSTAL CONN.
- REAR Al CRYSTAL CONN.
- SUBSTRATE HEATER CONN.
- SUBSTRATE HEATER ON
- COLD PLATE LN CONN.
- COLD PLATE LN ON
- FRONT Al FEED CONN.
- REAR Al FEED CONN.
- SUBSTRATE DRIVE MOTOR CONN.
- E-BEAM LEADS CONN.
- CONFIRM INTERLOCK INDICATORS ARE LIT
- CONFIRM COOLING WATER INDICATORS ARE LIT
- BAKE OUT SOURCES

3.8 Film Removal

The primary release layer used was a photoresist coating which was chosen because of its very smooth surface and its release characteristics. Good adhesion was exhibited during the deposition run when source power totaled 9.9 KW (e-beam 4.5 KW and boats 5.4 KW). The substrate speed was 3.4 ft/sec.

Test samples were removed from the substrate by framing the area with tape, scribing or cutting through the composite and pulling the film free from the surface of the release layer. In one instance the same AZ 1350 coating was used as a release layer for three separate runs.

Deposition rates were increased and the substrate speed was reduced to increase individual layer thickness. The substrate and release layer were exposed to source radiation for longer times and the release layer was not satisfactory under the higher temperature conditions. See Figure 6. The composite film peeled from the release layer during deposition. There was no delamination between layers within the composite. Expansion of the shim steel caused cracking in the release layer and resultant film defects.

Film which did not peel intact from the substrate was vacuumed from the release layer and/or removed in sodium hydroxide solution which removes the release layer as well as the aluminum composite film. Substrates were recoated. Release coatings were applied to the substrate with a Binks spray gun.

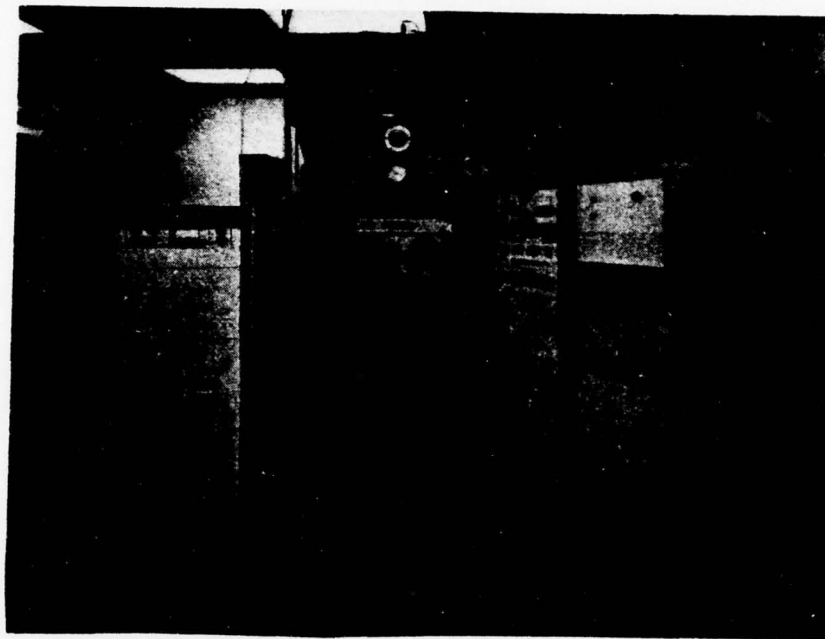


Figure 5. Prototype composite thin film deposition system.

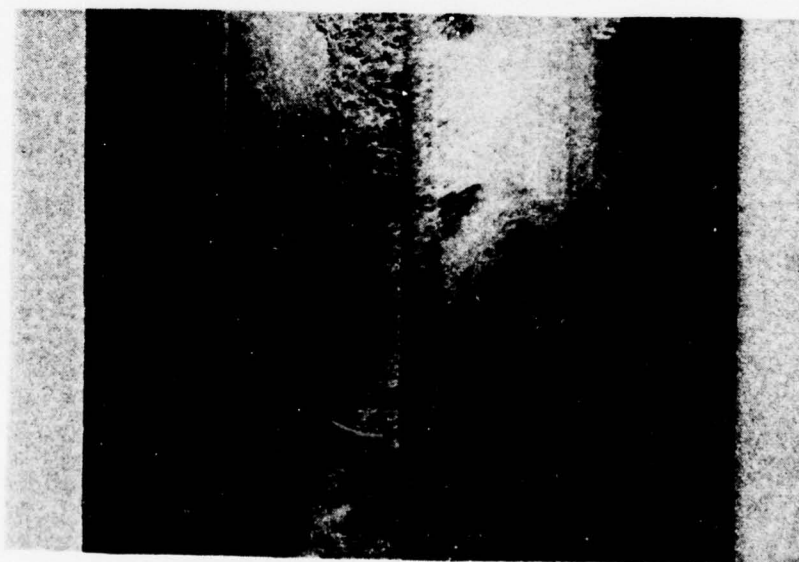


Figure 6. Substrate belt showing damage to release layer attributed to radiation from the electron-beam source.

The typical cure or bake-out prior to use was at 150° C for ½ hour.

AZ 111 resist was also used and the performance was similar to the AZ 1350. Two negative resists which were evaluated did not exhibit the desired smooth surface after baking. The best release observed was the removal of an alumina-aluminum composite sample from a strip of type 302 stainless shim steel (.001" thick). No release layer or treatment was used other than degreasing the stainless in acetone.

3.9 Heat Transfer

Since the primary mode of heat transfer in a vacuum is through radiation, the emissivity of the surfaces becomes an important factor. The cold plate and drive roller surfaces were untreated aluminum. Black anodization and flat black coatings were proposed as a means to increase emissivity. The surfaces were coated with a colloidal suspension of graphite. Heat transfer improved and was evidenced by comparison of the release layers after composite film deposition using the same deposition conditions, e.g., rates, substrate speed, and coolant.

However, when the rate for the high modulus material was increased and/or the substrate speed slowed, the release layer was damaged. Cracks developed in the release layer as the substrate expanded (thermal expansion). The composite film replicated the release layer surface which had the appearance of a dried creek bed.

4.0 Material Selection For Composite Deposition

A major goal in this multi-phase program is the development and deposition of a high specific strength material.

An ideal choice of materials from the point of view of their properties is one which combines high strength with low density and the capability for deformation and resistance to fracture. These characteristics are achievable by a composite matrix in which a high strength member is supported by an intimately bonded ductile member.

The majority of the composite depositions have been titanium-aluminum. Although these materials are attractive for vacuum deposition processes they are not necessarily the best choice for a high specific strength material pair.

Titanium is a desirable evaporant because its gettering action contributes to the pumping speed of the vacuum system.

Silicon carbide, alumina, and carbon have been suggested as possible choices for the high modulus material in the composite.

Silicon carbide and alumina have much higher moduli of elasticity than titanium.

The following two tables list selected materials and their values for modulus of elasticity and specific stiffness.

(Specific stiffness is the ratio of Young's modulus to density).

The data was taken from Materials Selector, Materials Engineering, Nov., 1977.

4.1 Modulus of Elasticity in Tension 10^6 psi

	High	Low
Silicon carbide	95	13
Alumina ceramic	50	30
Titanium and its alloys	18.5	11
Aluminum alloys 1000 series	10	10
Graphite, pyrolytic	4	
Graphite fiber	75	--

4.2 Specific Stiffness 10^6 in

	High	Low
Silicon carbide	819	
Graphite-epoxy composites	701	351
Alumina ceramic	357	
Aluminum alloys 1000 series	102	
Titanium and its alloys	101.1	69.6

The graphite-epoxy material differs in that it is already a composite.

4.3 Alternate Material Deposition

Deposition of carbon, SiC, and Al_2O_3 with Aluminum:

Vacuum evaporation of carbon, SiC and Al_2O_3 with aluminum required a modified substrate design. The high radiant heat output associated with evaporation of these materials requires a substrate with low thermal impedance to a heat sinking medium to control substrate temperature. Also, the lower deposition rate for these materials made it desirable to use a fixed substrate instead of a moving belt so that a film thick enough to strip could be deposited in a reasonable amount of time.

A 6" x 9" substrate was fabricated from 9/64" thick copper plate, to which was soldered copper tubing. The tubing was connected outside the vacuum system so that the substrate could be cooled with liquid nitrogen or maintained at a fixed temperature between 20° and 90°C by circulating water. The deposition surface of the copper plate was prepared by sanding and polishing with successively finer sanding grits until the final polishing which was done with 3 micron abrasive. The substrate was then cleaned and coated with photoresist to provide a smooth surface from which the evaporated film could be removed. Two such substrates were made to reduce the waiting time between successive deposition runs. Figures 7 and 8 show these substrates on which films have been deposited.



Figure 7. Alumina-aluminum layered composite. Alumina layer thickness increases from left to right. Aluminum layer thickness increases from right to left.

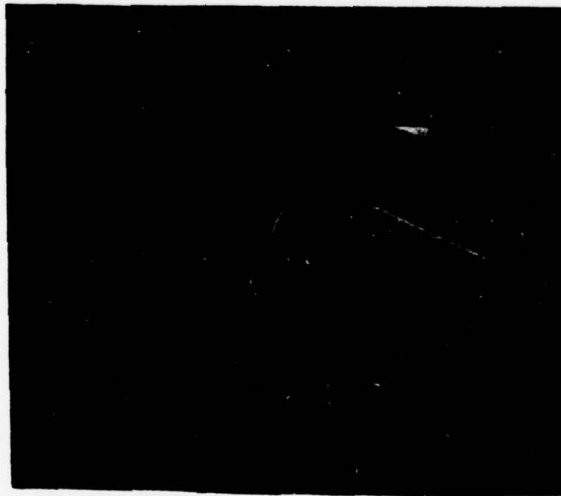


Figure 8. Silicon carbide aluminum layered composite. Silicon carbide layer thickness increases from left to right. Aluminum layer thickness increases from right to left.

The system was modified to the extent of installing a manually operated two position shutter. This shutter, shown in Figures 9 and 10, allows deposition alternately from two sources. The shutter was typically operated on a cycle such that the substrate received material from the aluminum side for 5 seconds while the e-beam source was blocked and then received material from the e-beam source for 10 seconds while the aluminum side was blocked. Another shutter was used to block the substrate entirely while the evaporant sources were stabilized.

The geometry of the evaporant sources and substrate result in a composition variation across the substrate so that in the case of aluminum-silicon carbide, one side has a higher ratio of aluminum to silicon carbide than the other. This variation is accentuated by the geometry of the two position shutter because the shutter requires a finite time (approximately 1 second) to move between the two positions. The crystal rate monitors are calibrated for a rate at the substrate center and thus corrections are needed for any other position on the substrate.

The thickness ratio correction source geometry is:³

$$\frac{t}{t_0} = \frac{1}{\left\{1 + \left(\frac{h}{d}\right)^2\right\}^2}$$

³ L. Holland, "Vacuum Deposition of Thin Film" Chapman and Hall 1963, p.145.

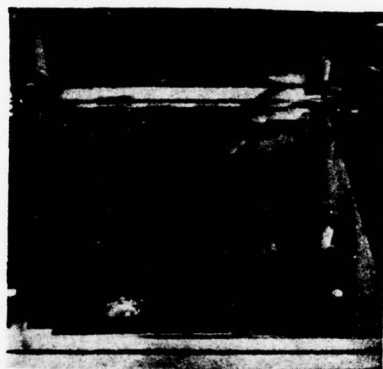


Figure 9. Shutter exposing e-beam hearth.

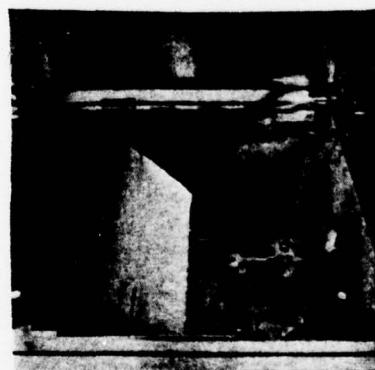


Figure 10. Shutter exposing resistance heated boats.

where h is the perpendicular distance between the small area source and the substrate and d is the lateral displacement of the substrate from a point directly over the source. For the source-substrate geometry used in this part of the work

$$\frac{t_1}{t_c} = 1.25 \quad \text{and} \quad \frac{t_2}{t_c} = 0.69 \quad \text{where}$$

t_1 is the thickness of the film at the edge of the substrate nearest the source, t_2 is the thickness of the film at the edge of the substrate furthest from the source and t_c is the thickness of the film at the center of the substrate. The subscript G refers to the source-substrate geometry correction.

The thickness ratio correction due to shutter mechanics varies according to the time the shutter is in each position. The correction is as follows:

Shutter Sequence (sec)	$\left(\frac{t_A}{t_B}\right)_1$	$\left(\frac{t_A}{t_B}\right)_C$	$\left(\frac{t_A}{t_B}\right)_2$
5:5	1.50	1.00	0.67
8:5	2.25	1.60	1.17
9:5	2.50	1.80	1.33
10:5	2.75	2.00	1.50
15:5	4.00	3.00	2.33

where t_A/t_B is the ratio of thickness of material A to material B and the subscripts 1, C and 2 refer to positions on the substrate nearest, in the center and furthest from source A respectively.

$$\text{minimum fraction A} = \frac{1}{1 + \frac{R_B \left(\frac{t_1}{t_C} \right)}{R_A \left(\frac{t_2}{t_B} \right)_2 \left(\frac{t_2}{t_C} \right)}}$$

$$\text{maximum fraction B} = \frac{1}{1 + \frac{R_B \left(\frac{t_2}{t_C} \right)}{R_A \left(\frac{t_A}{t_B} \right)_1 \left(\frac{t_1}{t_C} \right)}}$$

The variation in film composition from one side of the substrate to the other is frequently apparent from the visual appearance of the film as can be seen in Figures 7 and 8. In each case, a portion of the film peeled spontaneously from one end of the substrate. These were fairly typical results and in all cases it was the low-aluminum end of the film which peeled. The characteristics of the peeling were frequently very different as in Figures 7 and 8, but the reasons for this difference is not known. The peeling pattern is undoubtedly due to stress effects and the pattern suggests some influence from angle-of-incidence effects.

Two different Al-Ti films were characterized as described above. One film had a layer thickness estimated at 50 Å while the other was approximately 87 Å. The data is summarized in Table 1 below.

TABLE I

	Film A	Film B
Layer Thickness - Titanium	50 Å	87 Å
Layer Thickness - Aluminum	50 Å	121 Å
As deposited resistance	.082 ohm	.017 ohm
Annealed resistance	.257 ohm	.050 ohm

The most significant result of the temperature-resistance data is that both films increased in resistance by a factor of 3 and that no further changes in resistance occurred upon subsequent reheating. After the first excursion to 400°C, both films showed only small reversible resistance changes with temperature characteristic of metallic temperature coefficients of resistivity. After heating to 400°C, films which showed some ductility and strength became very brittle and fragile and tended to disintegrate even with careful handling. X-ray diffraction patterns of aluminum-titanium films showed essentially only the structures of aluminum and titanium both before and after annealing. After annealing, a very weak indication of the compound Al_3Ti was present. These results indicate that films consisting even of very thin layers of aluminum and titanium were undiffused and distinct as originally deposited. After annealing at 400°C for periods up to 15

minutes, sufficient diffusion occurred to alter the electrical and mechanical properties even through the formation of inter-metallic compounds was minimal.

Table 2 gives pertinent data for the series of deposition runs utilizing the source and substrate geometry described above. The nominal fraction of component thickness was calculated from the measured rate (averaged over the run) and the ratio of open shutter time for each source. The maximum and minimum ratios were calculated using the corrections described above for geometry and shutter effects according to the following formula, where R_A and R_B are the average measured deposition rates of components A and B respectively.

Table 3 shows the average layer thickness and total film thickness for this same group of films, based on deposition rates as determined by crystal thickness monitors. These values are necessarily approximate since the deposition rates sometimes varied substantially and the average rates used are therefore approximate calculations.

TABLE 2

Date	Source A	Source B	Rate A A/Sec	Rate B A/Sec	Open A sec	Shutter B sec	Time	Total Run Time min	Thickness Fraction A		
									Min	Nom	Max
12-17	Ti	Al	66	130	5	5		16.5	.16	.34	.66
12-20	Ti	Al	70	170	5	5		16.1	.13	.29	.52
12-21	Al ₂ O ₃	Al	21	60	10	5		12.2	.22	.41	.57
12-23	Al ₂ O ₃	Al	17	200	15	5		23.3	.10	.20	.38
1-3	Al ₂ O ₃	Al	14	120	10	5		40.0	.09	.19	.37
1-4	SiC	Al	21	125	var (5)	5		30.0	.06	.14	.31
1-6	SiC	Al	11	220	var (9)	5		29.2	.04	.08	.18
1-9	Al ₂ O ₃	Al	13	240	var (8)	5		20.8	.03	.08	.21
1-11	SiC	Al	17	186	10	5		23.7	.07	.15	.31
1-12	SiC	Al	12	193	10	5		31.7	.05	.11	.24
1-13	SiC	Al	15	100	10	5		38.0	.11	.23	.43
1-16	-	Al	-	236	-	-		8.3		0	

Table 3

Run Date	Average Layer Thickness		Total Film Thickness \bar{X}	Total Film Thickness mils
	A	B		
12-17	330	650	97,000	.38
12-20	350	850	115,900	.46
12-21	210	300	24,900	.10
12-23	255	1000	87,700	.35
1-3	140	600	118,400	.47
1-4	105	625	131,400	.52
1-6	99	1100	150,000	.59
1-9	104	1200	125,200	.49
1-11	170	930	104,300	.41
1-12	120	965	137,600	.54
1-13	150	500	98,800	.39
1-16	-	-	117,500	.46

5.0 Mechanical Properties - Experimental Methods*

The mechanical property measurements were conducted using the testing apparatus shown in Figure 11. This particular apparatus developed in the Georgia Tech Micromechanics Laboratory, employs a precision screw driven stage to displace one end of a specimen with the other end attached to a force transducer. A differential transformer monitors the displacement. The stage is driven by either of two constant speed synchronous motors which are easily changed to allow for changing the drive speed. Figure 12 shows a composite film tensile specimen mounted in the self-aligning swivel grip fixtures used for the measurements reported here.

Determination of tensile mechanical properties such as yield point and fracture stress generally require specimens which are free of edge and surface defects since such defects constitute stress raisers and seriously distort the results. This is particularly true for materials which exhibit brittle failure (little or no plastic deformation) which is typical of the composite materials fabricated on this program. It was extremely difficult to fabricate properly shaped tensile specimens which were defect free, due to the brittleness of the material, the difficulty of removing films from substrates, the presence of

* This section was taken in part from a report by B. R. Livesay, Applied Sciences Laboratory, Georgia Institute of Technology.

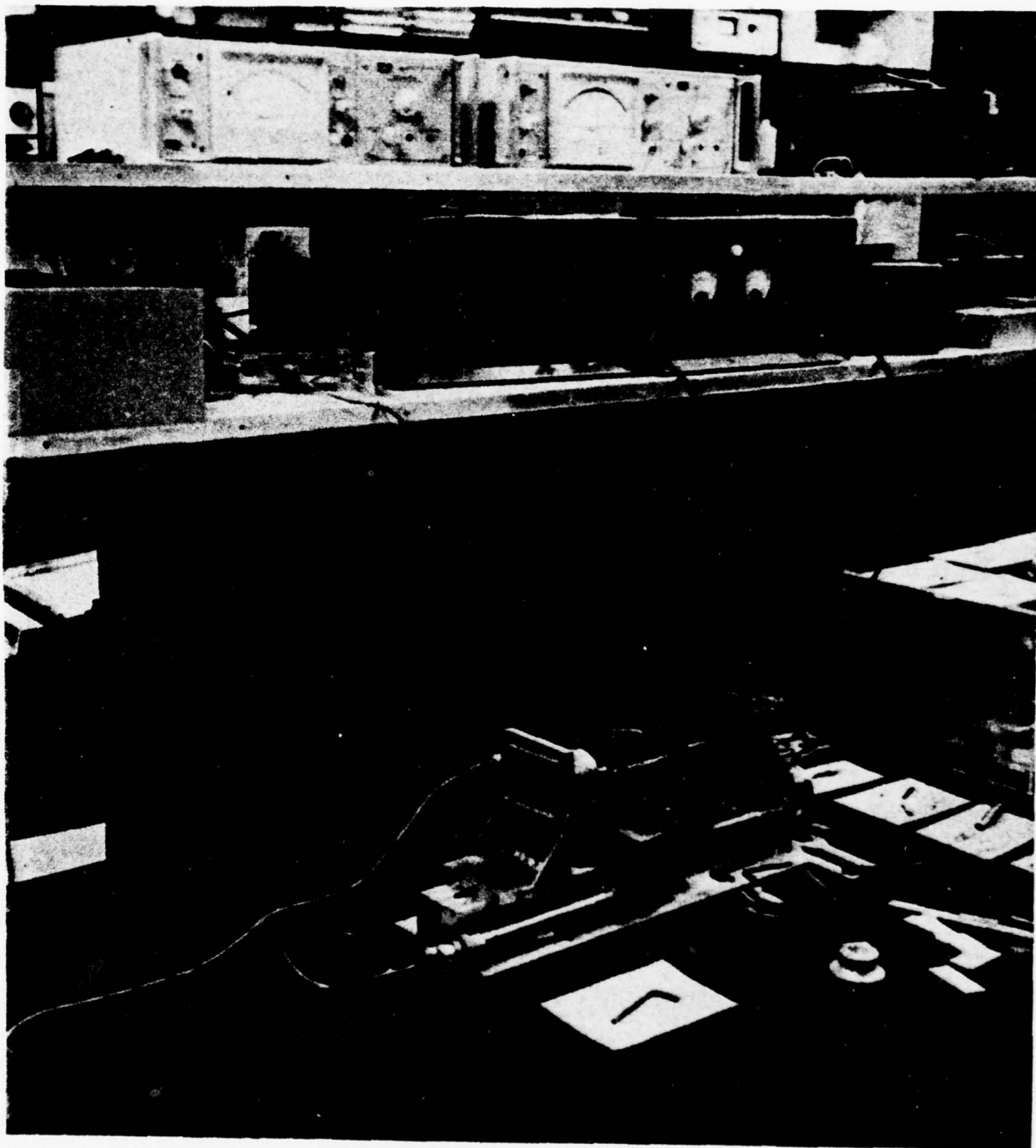


Figure 11. Measurement Apparatus Used to Determine Mechanical Properties of the Composite Specimens.

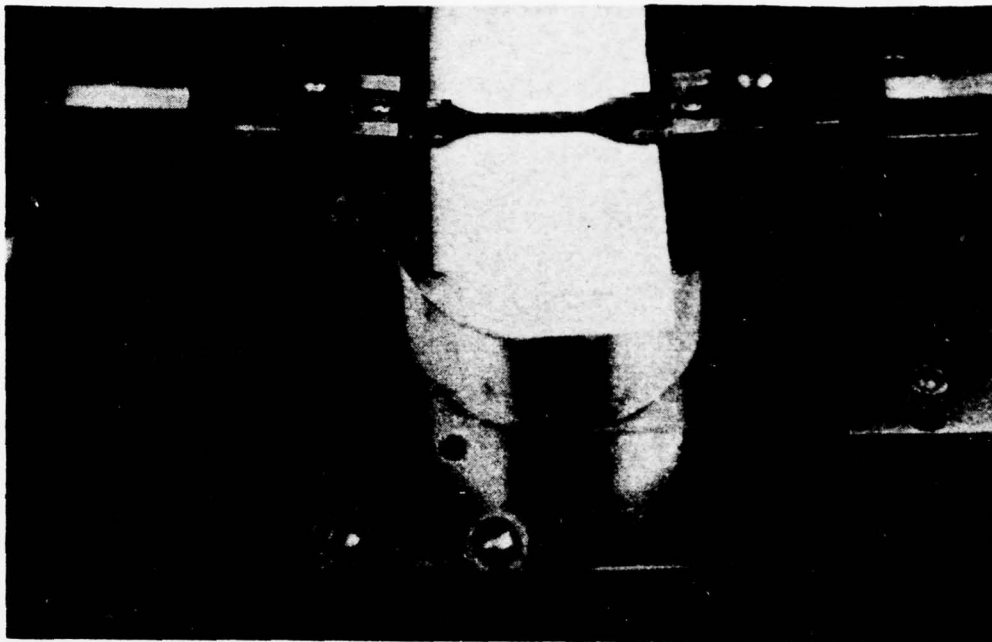


Figure 12. Tensile Specimen Mounted in Swivel Grips of Micromechanics Apparatus for Mechanical Test



Figure 13. Typical Internal Clamped Specimen Prior to Test.

pin-holes and cracks and in many cases the lack of substantial quantities of material. As a consequence, an internal clamp method was developed and utilized. This technique is described in detail along with results and analysis of the technique in subsequent sections.

The internal clamping method was used to determine strength of the brittle sheet materials involved here. This technique had earlier been postulated and employed at Sperry-Univac. The technique consists of attaching a film specimen to grips which are narrower than the specimen so that the edge of the specimen is not stressed. The specimen width is typically 3 times the grip width. Figure 13 shows a typical internally clamped specimen prior to test.

The use of the internal clamp technique proved to be useful for the specimens of this program. An example of the brittle nature of many of these materials is seen in Figure 14. The very slight bending involved in removing a test specimen from an adjacent piece of film spontaneously caused the film to shatter as shown. It was impossible to produce a standard tensile test specimen from this material. A specimen mounted in the testing machine discussed earlier is shown in Figure 15. In addition to decreasing the stress concentration at edge imperfections the internal clamp method provides for more convenient specimen mounting.

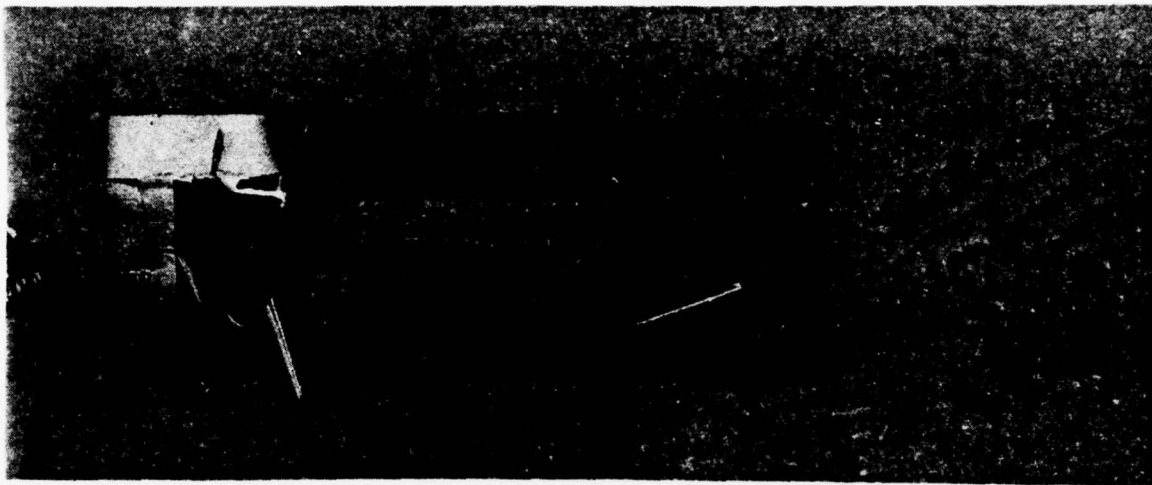


Figure 14. The Brittle Nature of Some of the Composites.

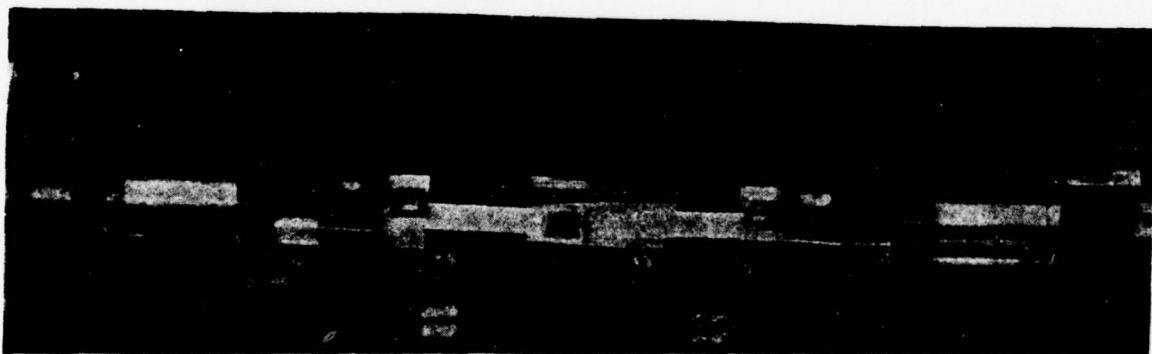


Figure 15. Internal Clamped Specimen Mounted in Swivel Grips

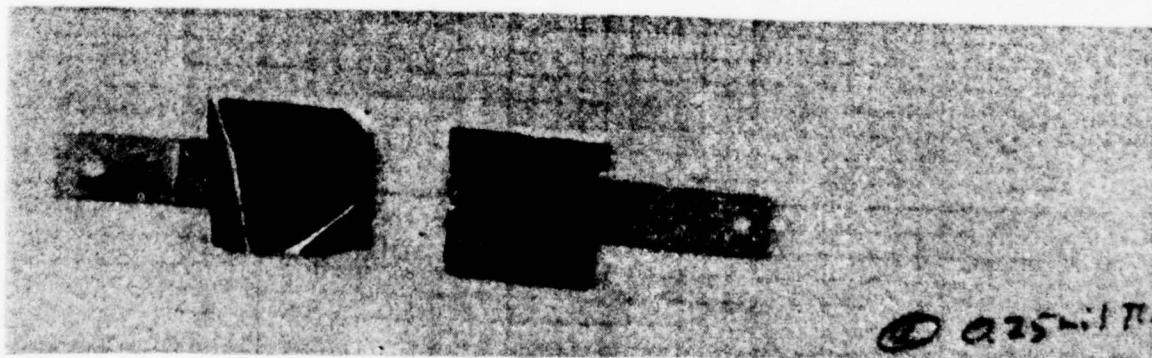


Figure 16. Fractured Composite Specimen Using Internal Clamped Fixtures

A fractured internal clamped specimen is shown in Figure 16. The value of specimen width to be used for calculation of ultimate tensile strength of an internally clamped specimen is not obvious and an experimental and theoretical analysis was performed to determine an appropriate geometrical factor.

Elastic modulus measurements were made with the same equipment described previously. Since longer specimens were needed to determine elongation with reasonable accuracy, not many samples were available which were suitable for good modulus measurements. The most reliable measurements were made on two Al-Ti films. Although the specimens fractured (or tore) at relatively low forces the initial slope of the curves permitted the Young's modulus to be computed. The swivel grips were removed to increase machine stiffness. The slopes of the curves were corrected for machine stiffness and other factors using curves taken for a thick Be-Cu dummy specimen; however it was not possible to account for small yielding within the metal-adhesive-metal interface. Therefore the modulus values will still tend to be low. Thickness of the test specimens was determined by SEM measurements performed by G. Lucas.

5.1 Analysis of the Internal Clamp Method

An experimental analysis of the internal clamp method was done by G. Lucas at MERADCOM using a photoelastic technique. An internally clamped specimen was prepared using the photoelastic material Lexan for the specimen and scaling the geometry of the

thin film specimen tests as closely as possible. Analysis of transmitted polarized light through the stressed sheet reveals the stress pattern within the specimen. Figures 17, 18, and 19 show the stress patterns at stress levels of 3100, 7430, and 12200 psi respectively. These patterns were analyzed for stress distribution and the results are shown in Figure 20, 21 and 22. The effective width is taken as the integrated area under the curve divided by the peak value of relative stress. Note that at higher stress levels, the effective width clusters closely around .75 times the tab width.

A theoretical analysis of the internal clamp method has been performed by E. J. Torok. This analysis shows that the effective width is a function of the ratio a/c where a is one-half the clamp width and c is one-half the clamp separation. For small a/c the effective width approaches a and as a/c becomes large the effective width approaches $2a$, consistent with the data of Lucas. The details of this analysis are given in Appendix A. The results reported in the following section are based on the effective width ($.75 \times$ clamp width) determined by Lucas.

5.2 Results of Mechanical Measurements

The results of measurements of tensile strengths of specimens tested by the internal clamp method are given in tables 4 and 5. Table 4 gives the results for six on which film thickness was measured at the fractured edge with an SEM. For the rest of the

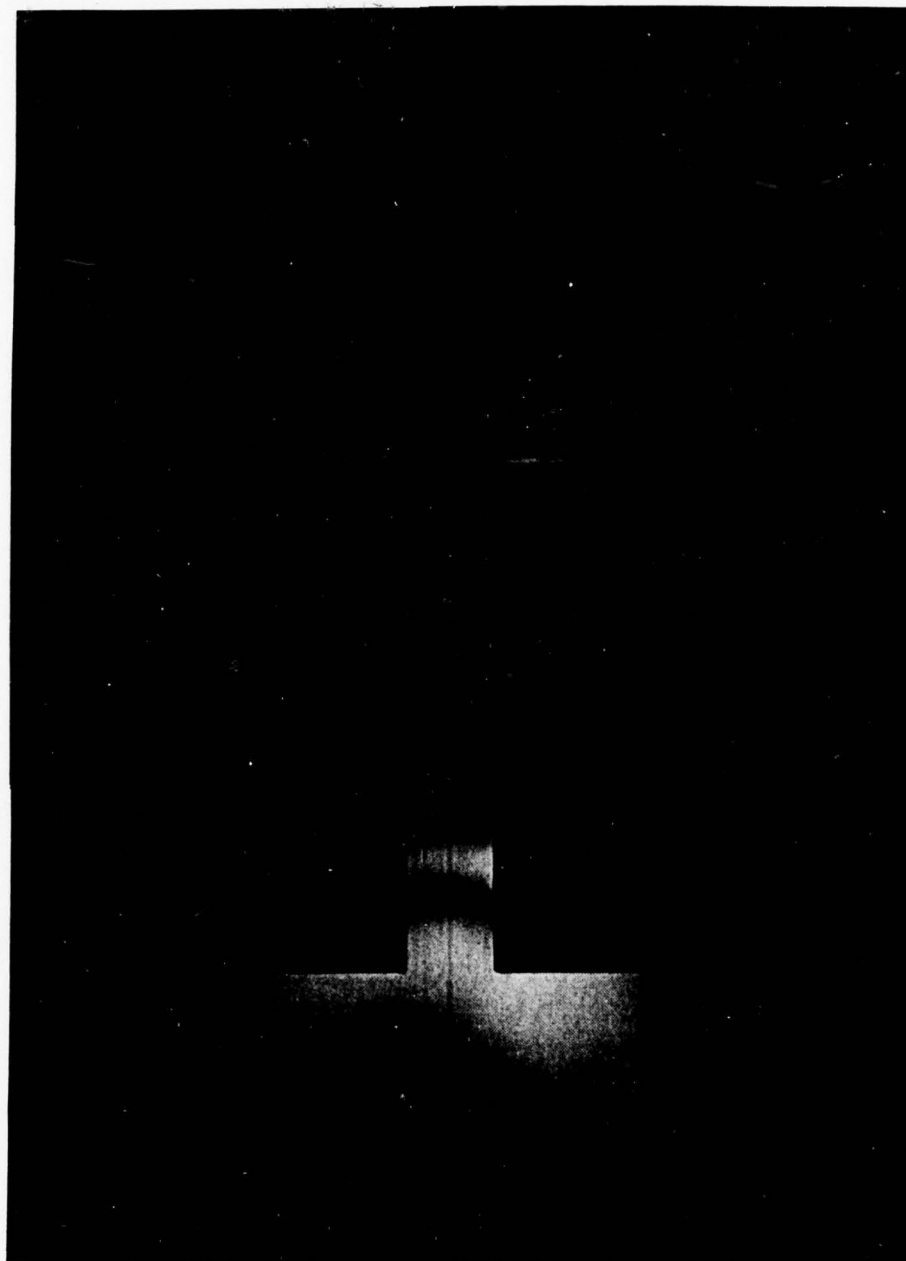


Figure 17: Photograph of Photoelastic Stress Distribution
for Internally Clamped Specimen

Material:	Lexan .020" x 5.0" x 5.0"
Force:	150 lbs
Max Stress:	3,100 psi
Tab Width:	2.0"
Total Specimen Width:	5.0"



Figure 18: Photograph of Photoelastic Stress Distribution for Internally Clamped Specimen

Material:	Lexan .020" x 5.0" x 5.0"
Force:	250 lbs
Max Stress:	7430 psi
Tab Width:	2.0"
Total Specimen Width:	5.0"

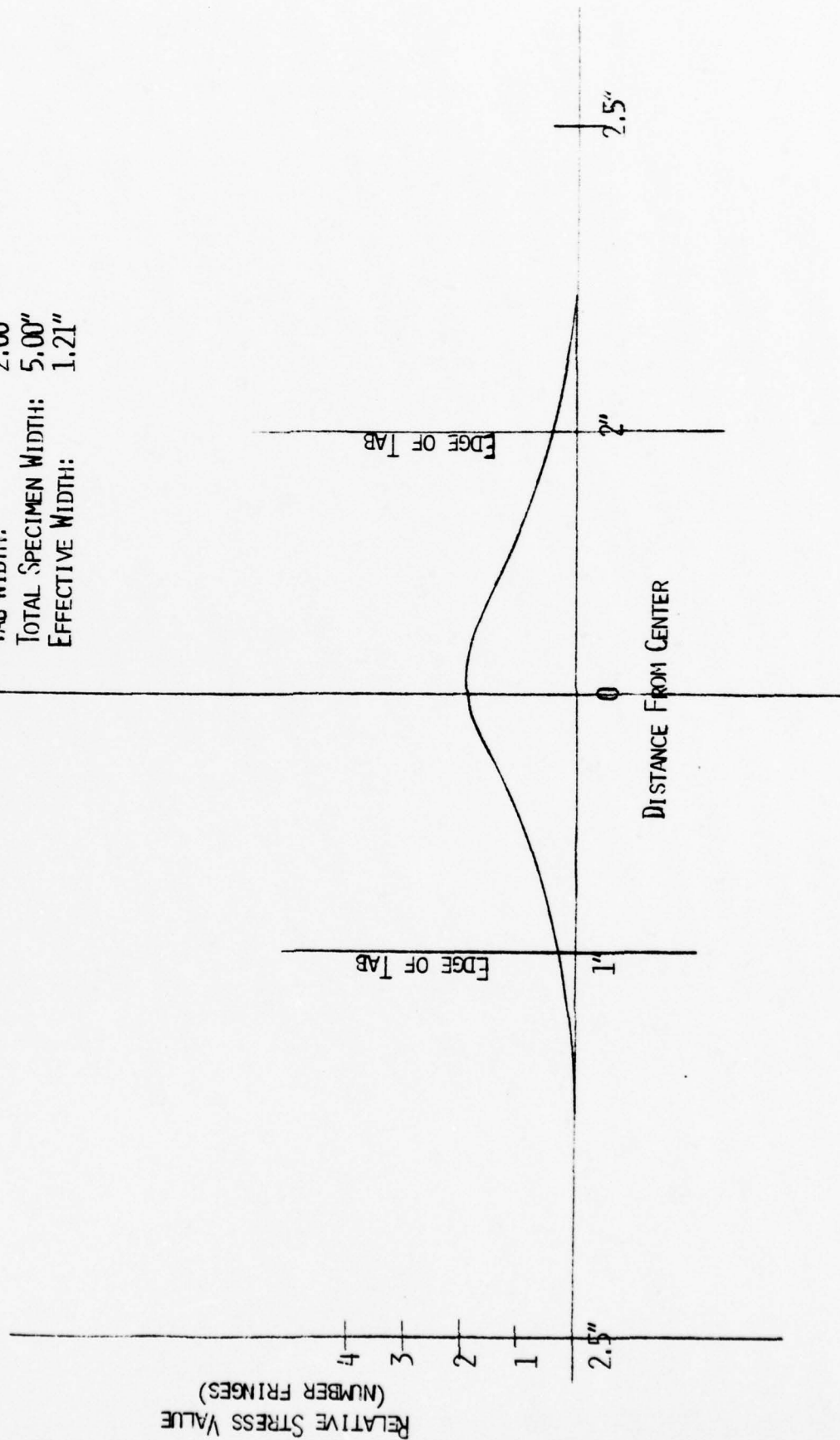


Figure 19: Photograph of Photoelastic Stress Distribution for Internally Clamped Specimen

Material:	Lexan .020" x 5.0" x 5.0"
Force:	375 lbs
Max Stress:	12,200 psi
Tab Width:	2.0"
Total Specimen Width:	5.0"

FIGURE 20:
GRAPH OF STRESS AS DETERMINED
BY PHOTOELASTICITY VS. DISTANCE
FROM CENTER LINE FOR MODEL OF THE
INTERNAL CLAMP TECHNIQUE

MATERIAL: LEXAN .020" THICK
5" X 5"
FORCE: 150 LBS
MAX STRESS: 3,100 PSI
TAB WIDTH: 2.00"
TOTAL SPECIMEN WIDTH: 5.00"
EFFECTIVE WIDTH: 1.21"



MATERIAL: LEXAN .020" THICK
 5" x 5"
 FORCE: 250 LBS
 MAX STRESS: 7450 PSI
 TAB WIDTH: 2.00"
 SPECIMEN WIDTH: 5.00"
 EFFECTIVE WIDTH: 1.68"

FIGURE 21:
 GRAPH OF STRESS AS DETERMINED
 BY PHOTOELASTICITY VS. DISTANCE
 FROM CENTER LINE FOR MODEL
 OF INTERNAL CLAMP TECHNIQUE

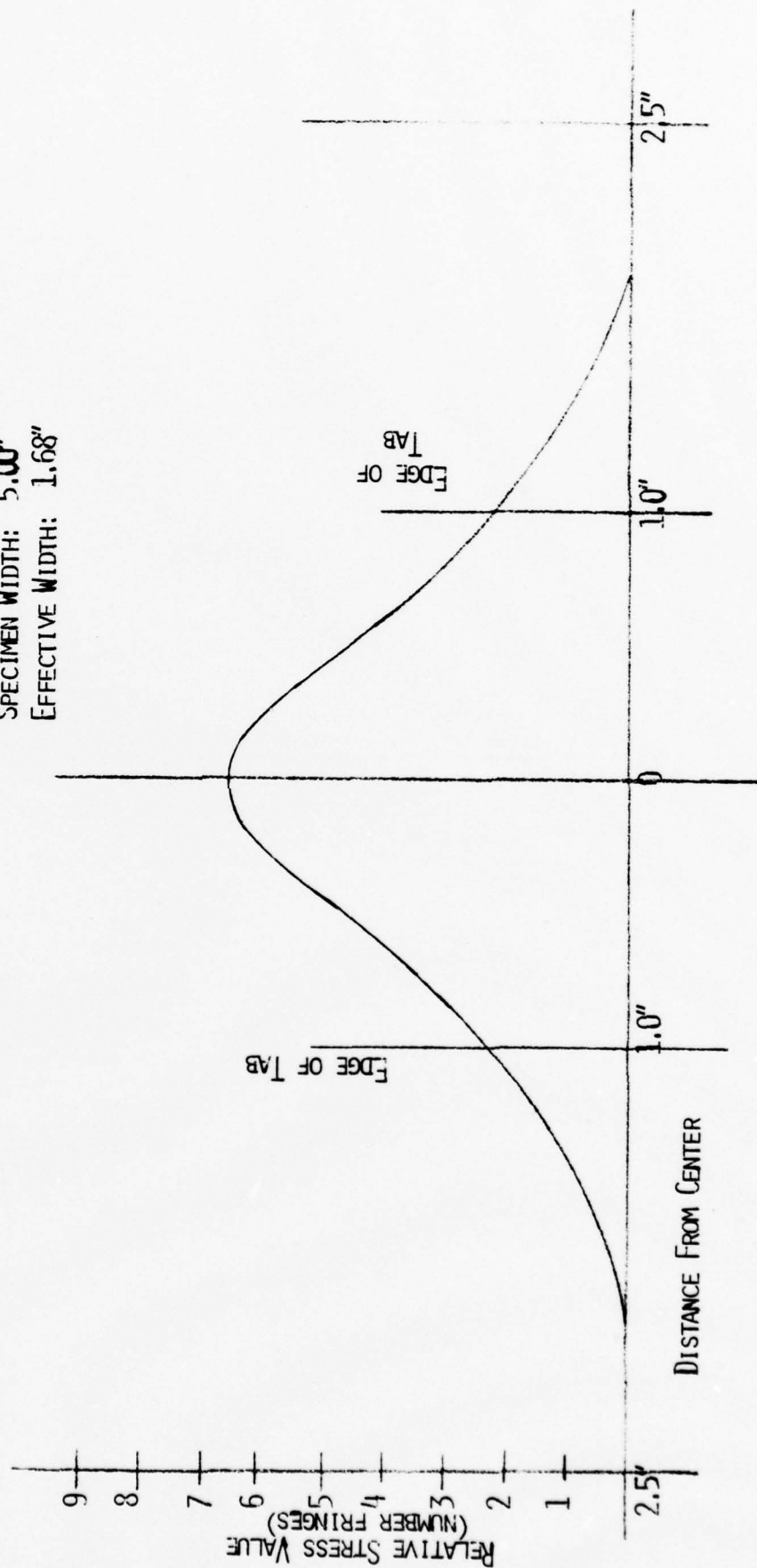


FIGURE 22:
 GRAPH OF STRESS AS DETERMINED BY
 PHOTOELASTICITY VS. DISTANCE FROM
 CENTER LINE OF SPECIMEN FOR MODEL
 OF THE INTERNAL CLAMP TECHNIQUE

MATERIAL: LEXAN, .020" THICK
 5" X 5"
 FORCE: 375 POUNDS
 MAX STRESS: 12,200 PSI
 TAB WIDTH: 2.00"
 SPECIMEN WIDTH: 5.00"
 EFFECTIVE WIDTH: 1.53"

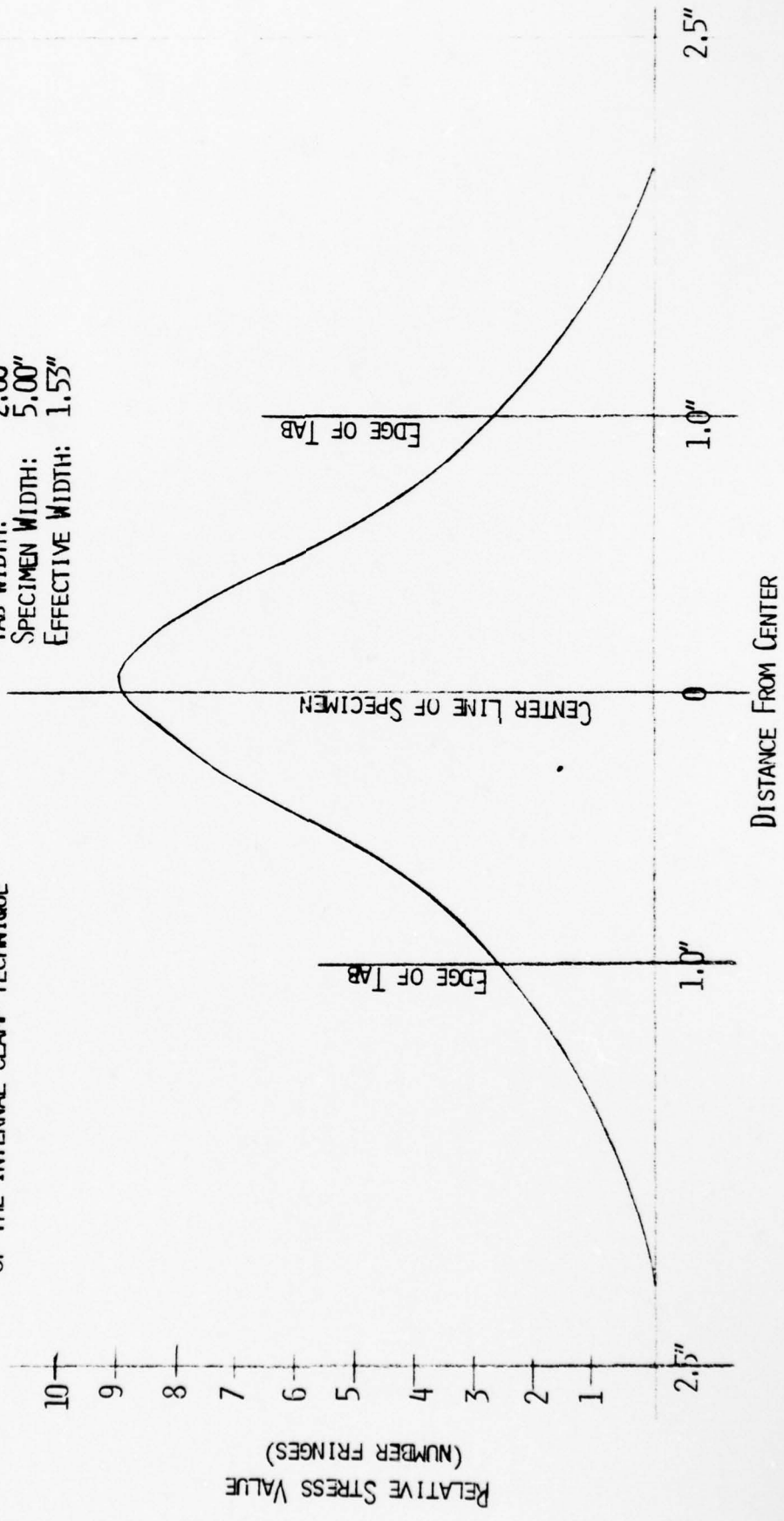


TABLE 4

Internal Clamp Method Fracture Strength: Thickness Measured by SEM

<u>Preparation Date</u>	<u>Identification</u>	<u>Thickness (10⁻³ in)</u>	<u>Average Layer Thickness (A) Al</u>	<u>Other</u>	<u>Approx No. of Layers</u>	<u>Fracture Load (lb)</u>	<u>Fracture Stress (psi)</u>
11-77	Al-Ti #1	.185	50	50	940	15.8	480,000
11-77	Al-Ti #1	.144	50	50	730	18.7	540,000
11-77	Al-Ti #2	.135	121	87	330	8.69	360,000
11-77	Al-Ti #2	.281	121	87	510	21.4	430,000
1-9-78	Al-Al ₂ O ₃ "hot sub- strate"	.480	1200	104	190	24.2	280,000
1-11-78	SiC-Al #2	.362	930	170	170	3.89	61,000

TABLE 5
Internal Clamp Method Fracture Strength

Preparation Date	Identification	Thickness (10-3 in)	Fracture Load		Average Layer	Thickness (A)		Fracture Stress (psi)
			(lb)			Al	Other	
11-77	Al-Ti #2	.25	4.31		121	87		97,000
11-77	Al-Ti #2	.25	11.9		121	87		270,000
11-77	Al-Ti #2	.25	5.39		121	87		120,000
12-3-77	Al-Ti "Some defects"	.15	2.77		121	87		100,000
12-3-77	Al-Ti	.10	1.32		121	87		75,000
12-3-77	Al-Ti "orange peel"	.15	.22		121	87		8,300
12-8-77	Al-Ti	.05	.44		121	87		50,000
12-20-78	Al-Ti Ti #1	.35	10.1		850	350		160,000
12-20-78	Al-Ti Ti #1	.35	2.64		850	350		43,000
12-20-78	Al-Ti- Al #3 Ti	.35	7.37		850	350		120,000
12-20-78	Al-Ti Al #3 Ti	.35	7.61		850	350		120,000
12-20-78	Al-Ti Al #3 Ti	.25	2.75		850	350		62,000
12-20-77	Al-Ti TiAl #1	.30	3.81		850	350		72,000
12-20-77	Al-Ti TiAl #1	.35	4.07		850	350		66,000
12-20-77	Al-Ti Al #2	.35	4.14		850	350		67,000
12-20-77	Al-Ti Ti #3 Al	.25	3.28		850	350		74,000
12-20-77	Al-Ti Ti #3 Al	.25	3.32		850	350		75,000
1-4-78	SiAl-AlSiAl-Al	1.65	27.1		850	350		93,000
1-9-78	Al-Al ₂ O ₃ "thickest Al ₂ O ₃)	.40	1.34		850	350		19,000
1-9-78	Al-Al ₂ O ₃	.40	.77		850	350		11,000
1-9-78	Al-Al ₂ O ₃ "hot substrate"	.90	22.44		1200	104		140,000

TABLE 5
Continued

Preparation Date	Identification	Thickness (10 ⁻³ in)	Fracture Load (lb)	Average Layer Thickness (A) Al Other	Fracture Stress (psi)
1-9-78	Al ₂ O ₃ -Al #3	1.00	4.95	1200 104	28,000
1-9-78	Al ₂ O ₃ -Al #3	0.45	2.66	1200 104	33,000
1-9-78	Al ₂ O ₃ -Al #4	0.65	5.94	1200 104	52,000
1-9-78	Al ₂ O ₃ -Al #5	0.75	12.2	1200 104	92,000
1-9-78	Al ₂ O ₃ -Al #5	0.65	8.1	1200 104	70,000
1-11-78	Al "from glass mirror"	1.00	14.3		81,000
1-11-78	SiC-Al #3	.40	3.39	930 170	48,000
1-11-78	SiC-Al #3	.35	4.11	930 170	66,000
1-11-78	SiC-Al #4	.50	5.94	930 170	67,000
1-12-78	SiC-Al #1 "Highest SiC"	.60	1.28	965 120	12,000
1-12-78	SiC-Al #1 "Highest SiC"	.45	.75	965 120	9,400
1-12-78	SiC-Al #2 "Middle SiC"	.45	.84	965 120	11,000
1-12-78	SiC-Al #2 "Middle SiC"	.40	.33	965 120	4,700
1-12-78	SiC-Al #3 "Lowest SiC"	.60	.22	965 120	2,100
1-16-78	Al only #1	.65	2.49		22,000
1-16-78	Al only	.20	1.84		52,000
1-16-78	Al only #3	.25	2.27		51,000

samples, listed in Table 5 thickness was measured with a machinist's micrometer. In the later case the measurements are subject to considerable error because of the difficulty of measuring thicknesses .001" or less with a micrometer. Average layer thickness, as determined by deposition rate monitors are also listed in the table. Specimen width is taken as 3/4 of the grip width or 0.177" as stated above.

Table 6 lists the data and results of measurements of elastic modulus. The stress-strain curves were obtained by B. Livesay using film thickness as measured with an SEM by G. Lucas.

TABLE 6
Elastic Modulus Measurements

<u>Specimen</u>	<u>Length</u>	<u>Width</u>	<u>Thickness</u>	<u>Measured Slope</u>	<u>Corrected Slope</u>	<u>E</u>
Al-Ti	2.89"	.177"	.000197"	.165 lb/mil	.177 lb/mil	14.7x10 ⁶ psi
Al-Ti	3.07"	1.97"	.000197"	.162 lb/mil	.1731 lb/mil	13.7x10 ⁶ psi

5.3 Film Properties - Resistance

Titanium-aluminum films were examined after deposition by means of resistance measurements. The film resistance after deposition was measured at room temperature and also during heating and cooling to approximately 400°C.

The purpose of these measurements on Al-Ti films was to determine the extent to which the as-deposited films consisted of distinct layers of aluminum and titanium. If the film did in fact consist of relatively undiffused layers, its resistance should be characteristic of two superimposed layers of those materials. If significant interdiffusion has occurred during deposition the resistance will be higher due to the existence of Al-Ti intermetallic compounds. In the former case, annealing will cause the resistance to increase while in the latter case, the resistance should be stable during annealing.

Resistance was measured, by means of an alumina strip onto which were attached nickel wires for making contact to the film. A standard 4-contact method was used to avoid errors due to contact resistance. A copper-constantan thermocouple was cemented to the fixture to monitor temperature. The test film was clamped to the fixture and the assembly was inserted into a tube furnace which had been previously stabilized at about 425°C. The resistance temperature curve was recorded on an X-Y plotter. The sample typically required about 5 minutes to reach thermal equilibrium, after which time no further changes in resistance were noted.

6.0 CONCLUSIONS

(1) Tooling:

The primary objective of phase II was the development of a composite thin film deposition system capable of relatively high deposition rates, e.g., one pound per hour. Sources and substrate tooling were installed with the capability of evaporating and collecting the multilayer composite titanium-aluminum at a one pound per hour rate.

The tooling and process have not been developed to the point of being directly applicable to a production facility.

(2) Problems related to the deposition rates:

The organic release layer was satisfactory at lower deposition rates. At higher rates the substrate and release layer were not compatible with the higher temperature vacuum environment. Non-uniform heating of the substrate (hotter in the center) reduced contact between the substrate and heat sinks which heightened the problem. Deposition was heat transfer limited.

Spitting from the e-beam source occurred at relatively low rates when the alternate high modulus materials alumina, silicon carbide and carbon were deposited. It was necessary to minimize spitting since the resulting holes in the composite films would greatly reduce its strength. Typical

rates for the alternate high modulus materials were 10 to 20 angstroms per second.

Carbon was not successfully evaporated in attempts to fabricate a carbon aluminum composite. The deposition rate was extremely low and spitting was excessive. Other investigators have been more successful in the evaporation of carbon.^{4,5}

(3) Thin film samples were deposited:

Titanium-aluminum, silicon carbide-aluminum and alumina-aluminum composites were successfully vapor deposited. In addition an aluminum only sample was prepared.

(4) Mechanical Tests:

Mechanical tests were performed to determine ultimate tensile strength and elastic modulus of composite films. Actual testing was done by Dr. Livesay at the Georgia Institute of Technology, however the calculated results are based on SEM thickness measurements and stress analysis of the internal clamp technique done by Lt. George Lucas at MERADCOM.

The results show very high tensile strengths for Al-Ti films. Tensile modulus of elasticity values have been measured which are somewhat higher than would be expected on the basis of the rule-of-mixtures.

⁴Preiswerk, P.R. and Lippman, M.E., "Physical Properties of Thin Films," Astro Corp., NASA Report, NASA CR-1972.

⁵Snowden, D.P. and Schoen, F.J., "The Compatibility of Carbon with Blood," Gulf General Atomic Company, San Diego, CA., March 29, 1972.

The high values of tensile strength obtained for Al-Ti films are evidence that composite materials with outstanding physical properties can be obtained by vacuum deposition in thin layers. The evidence for high strength Al-Al₂O₃ films is meager, but this result is probably related to the difficulty of fabricating and stripping composite films containing Al₂O₃ or SiC.

(5) Continuous layers:

There is evidence that the high modulus layers of a multi-layered composite film do not necessarily have to be continuous. The strength of a thin-film increases as the thickness decreases or as the layer approaches the point of discontinuity. Subsequent high strength layers would be expected to overlay discontinuities in preceding layers.

7.0 RECOMMENDATIONS

Composite film cost as well as the specific strength of the composite will have a major effect on production feasibility. The following recommendations are made:

- (1) Aluminum appears to be a good choice as the low modulus member of a composite pair. Aluminum is inexpensive, has low density and is easily evaporable. Sources and power supplies required for its deposition are proven and are low in cost.
- (2) The high temperature vacuum environment and the inherent heat exchange problems in vacuum recommend against the use of an organic release layer. Preferably the composite should be condensed directly onto the substrate.

- (3) Due to the anticipated high substrate temperature the material pair should not diffuse at high temperature. Al_2O_3 -Al or SiC-Al appear to be better choices in this respect than Ti-Al.
- (4) Process and equipment should be developed to upgrade (sinter and/or degas) low cost alumina and/or silicon carbide abrasives for use as the high modulus source material.
- (5) The rates of the high modulus member Al_2O_3 or SiC should be maximized (without spitting) and pellet feeds developed. Additional e-beam sources can be operated from a single power supply using individual gun control modules.
- (6) Equal thickness layers are not necessarily the best choice. Internal film stress appears lower when the high modulus member is thinner. Deposition of thicker layers of the low modulus member would be cost effective if film strength can be maintained.
- (7) Film removal at present is considered inadequate for a production process. The most attractive method still is the reduction in the radius of the substrate belt causing the composite film to peel from the substrate without breaking the vacuum.

The thicker composite, e.g., 0.8 mils, are easier to remove intact from the substrate. Additional processing and tooling development for film removal is required.

Appendix A

Analysis of Stress Distribution
in Measurements of Ultimate Tensile
Strength by the Internal Clamping
Technique

E. J. Torok

Abstract

An analysis of the stress distribution in films being measured by the internal clamping technique was made using Fourier analysis. An explicit closed expression was found that closely approximates the exact non-closed expression in Timoshenko. The maximum tensile stress in the film is very close to the force on the clamps divided by the width of the clamps and the film thickness. In order to avoid tearing the film, the sample should be wider than the clamps; the difference in widths should be greater than 1.5 times the gap between clamps.

Calculation of the Internal Clamping Stress

The starting point of our analysis is found in the book Theory of Elasticity by Timoshenko and Goodier, 2nd edition, 1951, page 50. They consider the two dimensional problem shown in figure 1b in which a beam of length L and width $2c$ is subjected to a compressive force $2q$ a uniformly distributed over a length $2a$ in the center of the beam. The compressive force is the same on the top and bottom of the beam. There is no force on the rest of the beam. By the use of Fourier series, they find that the y -component of stress at the center of the beam ($y = 0$) as a function of x , the distance along the beam, is given by:

$$\sigma_y = \frac{qa}{L} - \frac{4q}{\pi} \sum_{m=1}^{\infty} \frac{\frac{\sin M\pi a}{L}}{M} \left[\frac{\frac{M\pi C}{L} \cosh \frac{M\pi C}{L} + \sinh \frac{M\pi C}{L}}{\sinh \frac{2M\pi C}{L} + \frac{2M\pi C}{L}} \right] \cos \frac{M\pi X}{L} \quad (1)$$

Now this problem is the same as our problem except that the sign of the stress is reversed; that is, the sample is being stretched rather than compressed, so only the sign is different. The first step in solving equation 1 is to let the length of the sample to go to infinity, so the Fourier series becomes a Fourier integral. Let

$$V = \frac{M\pi C}{L} \qquad dV = \frac{\pi C}{L} = \frac{V}{M}$$

then

$$\sigma_y = \frac{4q}{\pi} \int_0^{\infty} \sin \frac{aV}{C} \left[\frac{V \cosh V + \sinh V}{\sinh 2V + 2V} \right] \cos \frac{VX}{C} \frac{dV}{V} \quad (2)$$

This integral can be solved numerically, but an explicit expression that is a close approximation is highly desirable. For this we replace the term in the brackets with an approximation:

$$\frac{V \cosh V + \sinh V}{\sinh 2V + 2V} \approx Ve^{-V} + \frac{e^{-V}}{2} \quad (3)$$

Note also that

$$\sin \frac{aV}{C} \cos \frac{VX}{C} = \sin \left(\frac{aV}{C} + \frac{X}{C} \right) V + \sin \left(\frac{a}{C} - \frac{X}{C} \right) V \quad (4)$$

Equation 2 becomes

$$\sigma_y \approx \frac{4q}{\pi} \int_0^{\infty} \left\{ \sin \left(\frac{aV}{C} + \frac{X}{C} \right) + \sin \left(\frac{a}{C} - \frac{X}{C} \right) V \right\} \left\{ e^{-V} + \frac{e^{-V}}{2V} \right\} dV \quad (5)$$

Evaluation of equation 5 requires solving integrals of the type

$$I = \int_0^{\infty} \sin \lambda V \frac{e^{-V}}{2V} dV \quad (6)$$

This is done by expanding $\sin \lambda V$ in a Taylor series, yielding

$$I = \frac{1}{2} \int_0^{\infty} \left\{ \lambda - \frac{\lambda^3}{3!} V^2 + \frac{\lambda^5}{5!} V^4 - \frac{\lambda^7}{7!} V^6 + \dots \right\} e^{-V} dV$$

Now since $\int_0^{\infty} X^n e^{-X} = n!$,

$$I = \frac{1}{2} \left\{ \lambda - \frac{2!}{3!} \lambda^3 + \frac{4!}{5!} \lambda^5 - \dots \right\}$$

$$= \frac{1}{2} \left\{ \lambda - \frac{\lambda^3}{3} + \frac{\lambda^5}{5} - \frac{\lambda^7}{7} + \dots \right\}$$

$$= \frac{1}{2} \tan^{-1} \lambda \quad (7)$$

With the use of equation 7, equation 5 becomes

$$\sigma_y \approx \frac{2q}{\pi} \left[\frac{\frac{a+C}{C}}{1 + \left(\frac{a+X}{C}\right)^2} + \frac{\frac{a-X}{C}}{1 + \left(\frac{a-X}{C}\right)^2} + \frac{1}{2} \tan^{-1} \left(\frac{a+X}{C}\right) + \frac{1}{2} \tan^{-1} \left(\frac{a-X}{C}\right) \right]$$

(8)

This is the desired result.

Comparison of Approximate and Exact Solutions

Timoshenko and Goodier (ibid) reprint the results of L.N.G. Filon, who evaluated equation 1 exactly for the case where the dimension a is very small (i.e. concentrated force $P = 2qa$).

This case where $a \ll C$ can be found from our approximate solution by differentiating equation 8 with respect to a . The result is

$$\sigma_y = \frac{2q}{\pi C} \left[\frac{3}{1 + \left(\frac{x}{C}\right)^2} - \frac{4x^2/C^2}{1 + \frac{x^2}{C^2}} \right] \quad (9)$$

The exact (eq 1) and approximate solution are compared in figure 2. Note that the two curves are very close, indicating that equation 8 is a close approximation to the exact solution which can only be evaluated numerically.

Discussion of Stress Distribution

Figure 3 shows the stress in the case where $a = 2C$, i.e. the separation of the clamps is half the width of the clamps. A central portion of the film between the clamps, is under tension. Near the edge of the clamps the tension falls off, and a short distance outside the clamps the stress is compressive. This reversal of sign was also found in Filon's exact solution for the case $a = 0$ as reported in Timoshenko, (the curve of figure 2). The distribution for the clamps infinitely close together is a square wave, illustrated by the broken line in figure 3. Separating the clamps just changes the stress somewhat near $x = a$, (i.e. filters the square wave slightly).

In measuring the ultimate tensile strength of a thin film, the quantity of importance is the maximum tension anywhere in the film as a function of load on the clamps. The spot with the maximum tension will rupture first, causing the whole film to tear. This study shows that the maximum tension is always at least as high as that calculated by the force on a clamp divided by the clamp width and the film thickness.

THE X-COMPONENT OF STRESS

The X component of stress when $y = 0$ is given (by similar reasoning) as

$$\sigma_x = \frac{4q}{\pi} \int_0^{\infty} \sin \frac{av}{c} \left[\frac{V \cosh V - \sinh V}{\sinh 2V + 2V} \right] \cos \frac{Vx}{c} \frac{dV}{V}$$

As before, an analytic expression can be obtained for the stress if the quantity inside the brackets is approximated by a more manageable expression; for this we use $0.2V^2e^{-V}$. The result is

$$\sigma_x = \frac{8q}{5\pi c} \left\{ \frac{a+x}{\left[1 + \left(\frac{a+x}{c}\right)^2\right]^2} + \frac{a-x}{\left[1 + \left(\frac{a-x}{c}\right)^2\right]^2} \right\}$$

This expression is plotted in figure 4 for the case $a = 2c$. We see that σ_x is tensile when $|x| < a$, becomes zero at almost exactly the point $x = a$, and is compressive for x larger than that.

The compressive stress σ_x when $|x| > a$ (i.e. outside the width of the clamps) is associated with the tensile y - component, σ_y , there. If the sample being tested is a thin film, having thickness much less than a or c , then

the sample will buckle under compressive stress. This explains the wrinkling sometimes observed in thin film samples being tested by this method. This slight buckling reduces the compressive stress and also the tensile stress when $|x| > a$. The effect is to confine the tensile stress σ_y to the region $|x| < a$. Thus for thin films the stress σ_y is uniform and confined to the region inside the width of the clamps; this fact suggests that one may measure Young's modulus in thin films with the internal clamping method.

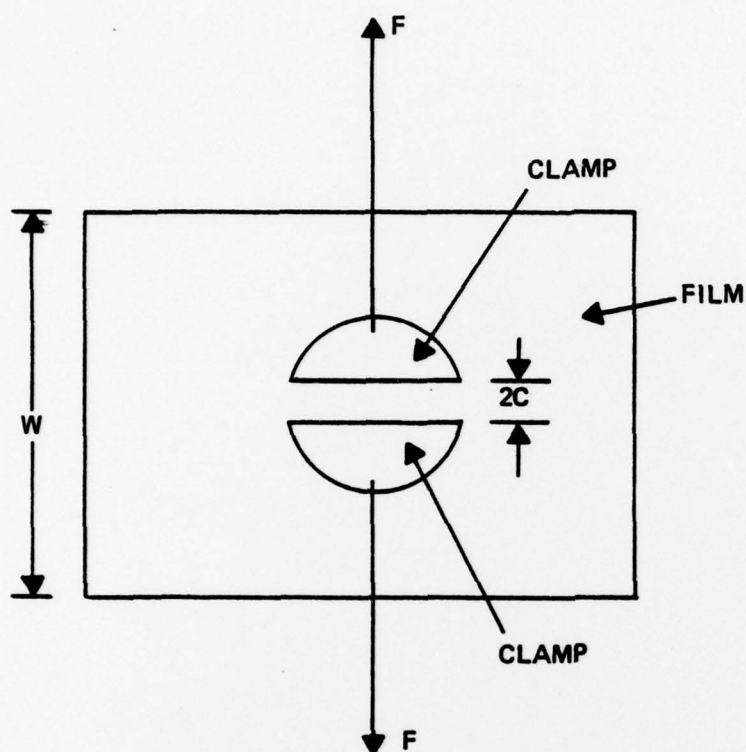


Fig. 1a. Film Being Tested for Ultimate Tensile Strength by the Internal Clamping Technique

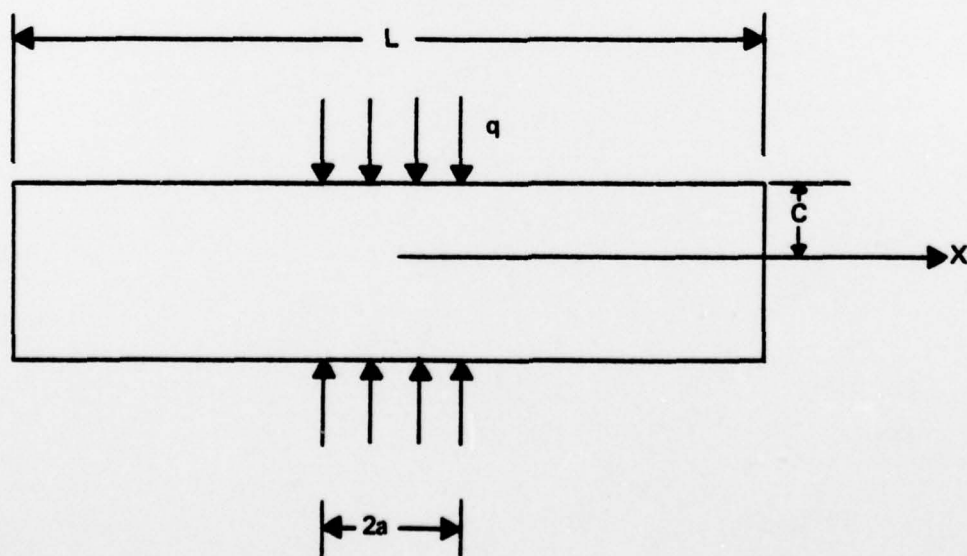


Fig. 1b. Beam Being Compressed by Square Wave Forces

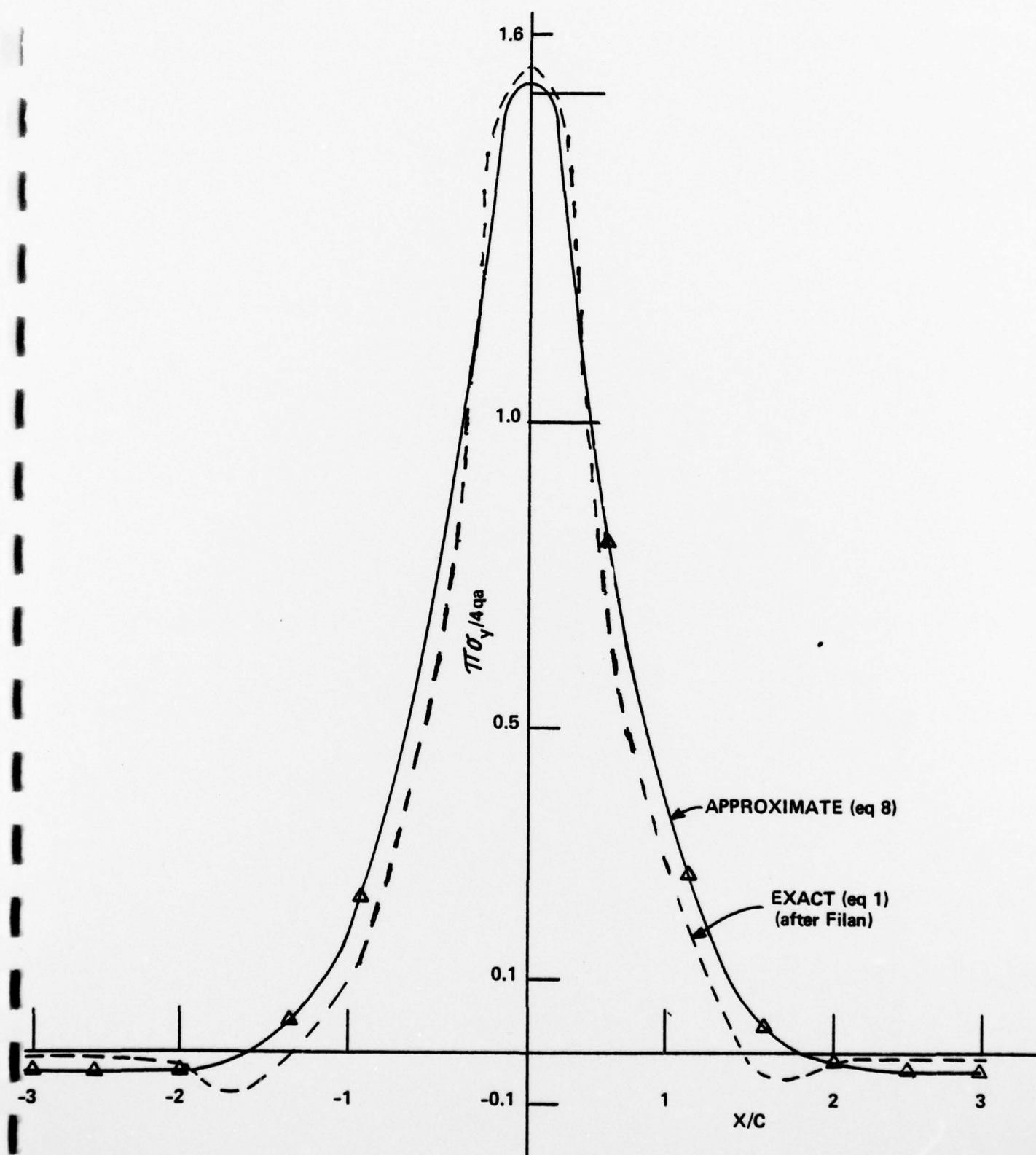


Fig. 2. Comparison of Exact and Approximate Stress Curves when $a \ll c$

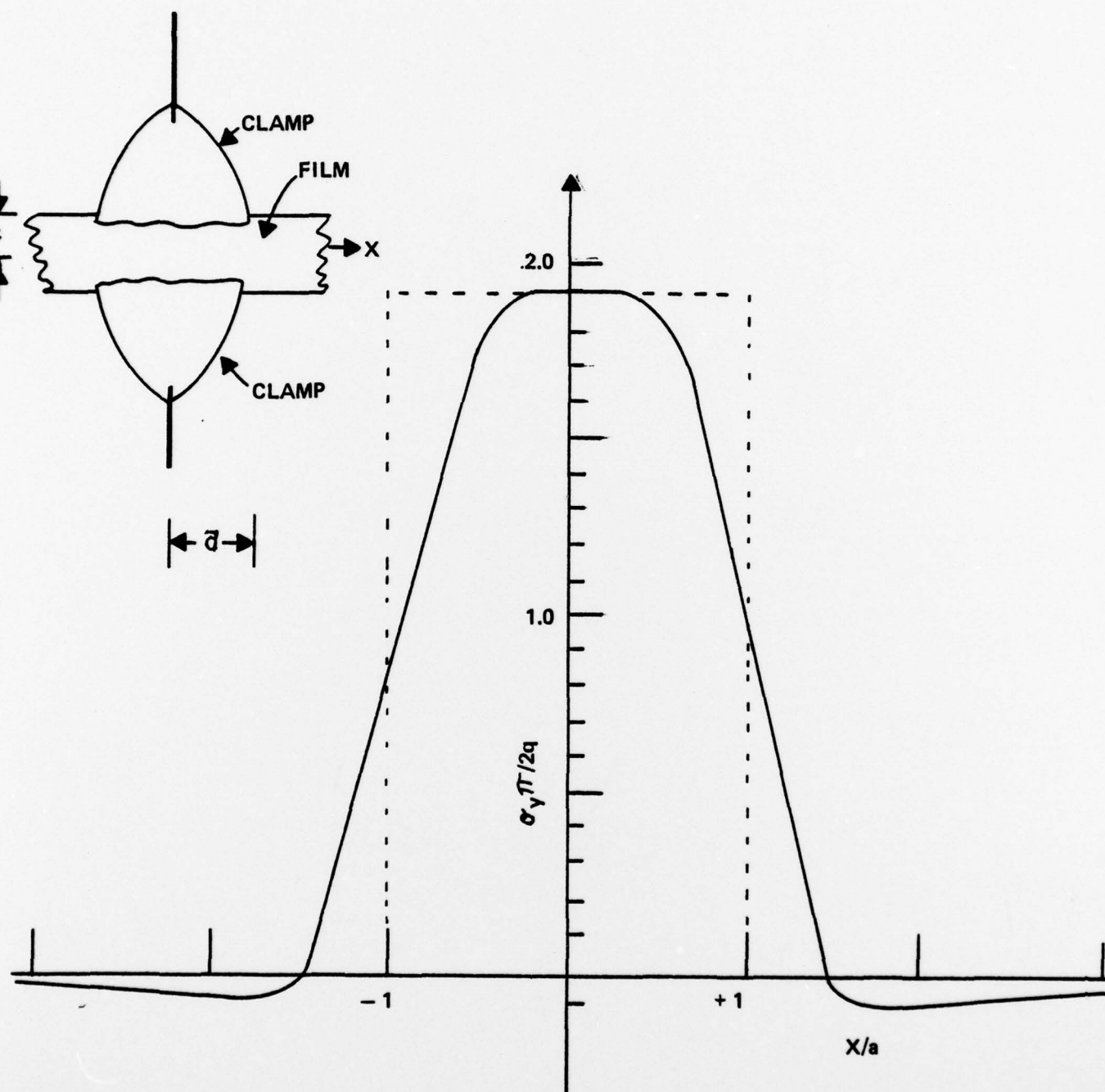


Fig. 3. Stress σ_y when $y = 0$ as a Function of Distance X/a when $a = 2C$

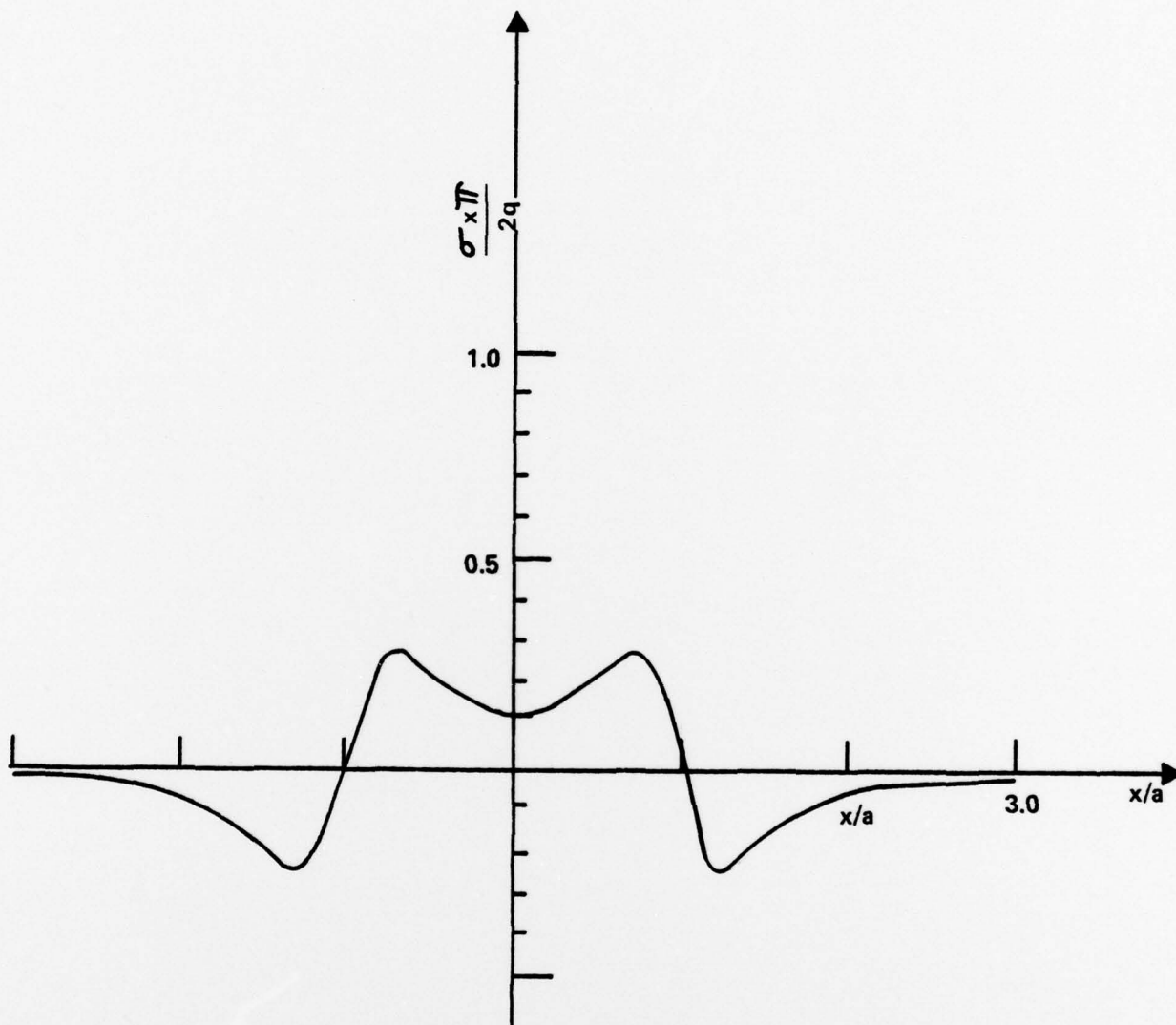


Figure 4. The X-Component of Stress for the Case $a = 2c$

Appendix B
Distribution of Report

<p>1 MERADCOM Fort Belvoir, VA 22060 Commander, DRDME-Z Technical Director, DRDME-ZT Assoc Tech Dir/R&D, DRDME-ZN Assoc Tech Dir/Engrg & Acq DRDME-ZE Spec Asst/Matl Asmt, DRDME-ZG Spec Asst/Tech Asmt, DRDME-ZK CIRCULATE</p>	<p>1 Commander, Naval Facilities Engineering Command Department of the Navy ATTN: Code 032-A 200 Stovall St Alexandria, VA 22332</p>
<p>1 Chief, Ctrmine Lab, DRDME-N Chief, Engy & Wtr Res Lab DRDME-G Chief, Elec Pwr Lab, DRDME-E Chief, Cam & Topo Lab DRDME-R Chief, Mar & Br Lab, DRDME-M Chief, Mech & Constr Eqpt Lab DRDME-H Chief, Ctr Intrus Lab, DRDME-X Director, Product A&T Directorate DRDME-T CIRCULATE</p>	<p>1 Director Lewis Directorate US Army Air Mobility R&D Lab ATTN: SAVDL-LE 21000 Brook Park Rd Cleveland, OH 44135</p>
<p>1 Tech Reports Ofc, DRDME-WP</p>	<p>1 Director, Technical Information Defense Advanced Research Projects Agency 1400 Wilson Blvd Arlington, VA 22209</p>
<p>1 Security Ofc, DRDME-S</p>	<p>1 Director Langley Directorate US Army Air Mobility R&D Lab ATTN: SAVDL-LA Mail Stop 266 Hampton, VA 23365</p>
<p>1 Tech Library, DRDME-WC</p>	<p>1 Department of the Navy Naval Air Systems Command ATTN: Mr. W.T. Highberger, AIR-52031D Washington, DC 20360</p>
<p>1 Director, Programs & Analysis Dir DRDME-U</p>	<p>1 Artech Corporation ATTN: Mr. Henry Hahn 2816 Fallfax Drive Falls Church, VA 22042</p>
<p>1 Pub Affairs Ofc, DRDME-I</p>	
<p>1 Ofc of Chief Counsel, DRDME-L</p>	

15	Mat Tech Lab, DRDME-V	1	Engineering Experiment Station Georgia Institute of Technology ATTN: Dr. B.R. Livesay Atlanta, GA 30332
1	Director US Army Industrial Base Engineering Activity Rock Island Arsenal ATTN: DRXIB-MT Rock Island, IL 61202	15	Defense Document Center Cameron Station Alexandria, VA 22314
1	Director US Army Materials and Mechanics Research Center ATTN: DRXMR-STL, Tech Library DRXMR-PT Watertown, MA 02172		
	Air Force Materials Laboratory Manufacturing Technology Div		
1	ATTN: AFML/LTM		
1	AFML/LTN		
1	AFML/LTE		
	Wright-Patterson Air Force Base, OH 45433 CIRCULATE		